Recognition of Cancer using Random Forests as a Bag-of-Words Approach for Gastroenterology

Sara Isabel Moreira Francisco

Supervisor: Ricardo Sousa, PhD

Co-Supervisor: Miguel Coimbra, PhD

Mestrado em Engenharia Biomédica

June, 2015

Faculdade de Engenharia da Universidade do Porto

Recognition of Cancer using Random Forests as a Bag-of-Words Approach for Gastroenterology

Sara Isabel Moreira Francisco

Dissertation submitted to Faculdade de Engenharia da Universidade do Porto

Mestrado em Engenharia Biomédica

June, 2015

Abstract

Cancer in the gastrointestinal tract is one of the deadliest diseases worldwide. This type of cancer has few symptoms in its early stages, thus its early diagnosis is essential to improve the survival rate and leads to a better prognosis. Medical imaging processing technologies for cancer diagnosis have been evolving during the last century, especially endoscopes. They allow the acquisition of images of the tissues on the gastrointestinal tract with good resolution. Techniques to analyze these images have been developed and have been used by Computer Aided Diagnosis (CAD) systems.

In gastroenterology, CAD systems techniques have allowed physicians to analyze endoscopic images using this tool as a first or second opinion, or even as an educational program. Cancer recognition in the gastroenterology tract is a complex challenge in which only trained physicians have a high rate of success. Some pattern recognition solutions covering this issue have already been explored in the past. However, these solutions need to be adjusted or self-tailored and are unable to automatically learn the best features to describe the data. In our approach, we extract pixel-based information (patches) and generate a Bag of Words (BoW) using Random Forests (RF) to hierarchically cluster and describe the patterns on the images.

Our experimental study is made over a dataset of chromoendoscopy images, to which we studied the tuning of all the relevant parameters. Our methodology presented its optimal performance for the following processing parameters: images converted to grayscale; patches with 5×5 pixels are descriptive enough; the methodology performs better when using just a part of the patches, even when chosen randomly; the number of trees in the forest and the number of node per tree influences the performance of the methodology, providing better performance for intermediate values (when computational complexity is taken into account); one-versus-all strategy was used to classify with Support Vector Machines (SVM). Finally we evaluated our proposed methodology from a global point of view, obtaining $23.07 \pm 2.83\%$ of mean error. This is a competitive result, when compared to the standard methodologies used in gastroenterology and a methodology suitable to be used in a medical environment, with near-real time feedback to physicians.

Keywords: Gastroenterology; Computer Vision; Random Forests; Bag of Words.

Resumo

O cancro no trato gastrointestinal é uma das doenças mais mortais em todo o mundo. Este tipo de cancro tem poucos sintomas nos primeiros estadios da doença, aquando o diagnóstico é essencial para maior probabilidade de sobrevivência dos pacientes. As tecnologias de diagnóstico deste cancro evoluíram ao longo do último século, especialmente os endoscópios. Eles permitem a obtenção de imagens dos tecidos do trato gastrointestical com uma resolução e qualidades suficientes para serem analisadas utilizado sistemas de diagnóstico assistido por computador (CAD).

Em gastroenterologia, os sistemas CAD têm tido um papel importante na avaliação de imagens de endoscopia, como ferramentas de primeira ou segunda opinião para os médicos, ou mesmo como um programa de aprendizagem. O reconhecimento de cancro no trato gastrointestinal é um desafio complexo onde apenas os médicos especialistas são capazes de fazer um diagnóstico altamente preciso. De forma a colmatar as lacunas existentes, algumas soluções para o reconhecimento de padrões têm sido exploradas. No entanto, para que estas soluções sejam viáveis em gastroenterologia, é necessária a intervenção de investigadores para cada novo tipo de imagens. As metodologias existentes não são capazes de identificar e descrever automaticamente os padrões e/ou as características mais discriminativas das imagens. A solução que propomos neste trabalho visa apresentar uma alternativa que vá ao encontro das anteriores limitações.

A nossa metodologia extrai informação diretamente dos pixeis, sob a forma de patches, gera um *Bag of Words* utilizando *Random Forests*, a partir do qual é feito um *clustering* hierárquico, quantificando os diferentes padrões existentes nas imagens. Esta quantificação permite criar um histograma por cada imagem, o qual tratamos por Vocabulário. O Vocabulário é a entrada para a etapa da classificação.

Este trabalho apresenta a metodologia utilizada e o respetivo estudo experimental para um problema multi-classe, tendo como objeto de estudo um conjunto de imagens obtidas por cromoendoscopia. O estudo contemplou, além de uma apresentação detalhada de toda a abordagem, uma escolha dos melhores parâmetros. Após este estudo, concluímos que esta metodologia é capaz de captar melhor a informação relevante quando as imagens são convertidas para escalas de cinzento; os patches com 5 pixels de lado extraem informação suficiente para este contexto; o desempenho da metodologia é superior quando utilizados apenas alguns dos patches, ainda que escolhidos de forma aleatória; o número de árvores na floresta e o número de nós por árvore influenciam o desempenho do método, permitindo o melhor desempenho para valores intermédios (quando temos em conta o custo computacional); a estratégia *one-versus-all* foi utilizada garantindo robustez na classificação de 3 classes, onde utilizamos *Support Vector Machines*. Finalmente, avaliamos a metodologia que propomos de um ponto de vista global, obtendo $23.07 \pm 2.83\%$ de erro médio, utilizando os melhores parâmetros para o dataset em questão. Este resultado é competitivo quando comparado com as metodologias aplicadas atualmente em gastroenterologia. A metodologia é, ainda, aplicável quase em tempo real, sendo adequada para uma utilização em ambiente médico.

Keywords: Gastroenterologia; Visão por Computador; *Random Forests*; *Bag of Words*.

Agradecimentos

Sou uma pessoa de agradecimentos. Gosto da palavra *obrigada*, já que geralmente é mais fácil não ajudar e que acho o exercício da gratidão essencial. Assim, hoje quero agradecer à informalidade desta secção que me permite não ser científica e pelo contrário, prática e emocional, agradecendo a todos os que permitiram que eu chegasse ao fim deste percurso ainda com alguma sanidade mental (coisa que duvidei ser possível até hoje).

Antes de mais, agradeço aos orientadores deste trabalho. Ao Ricardo que me acompanhou, ainda que às vezes não compreendendo as minhas razões para encarar este trabalho como um fim em vez de um princípio. E ao Miguel, que me integrou tão bem, permitiu contactar com um mundo que não é o meu, passando nas entrelinhas uma das minhas mensagens favoritas: trabalhar com amizade e em equipa é sempre mais fácil.

Agradeço aos amigos que se mantiveram fortíssimos e presentes mesmo com todas as minhas promessas de tempo falhadas; agradeço à Filipa, ao Francisco, aos Maneis, à Carla, à Inês, à Joana, à Sofia, ao Fernando, ao Gonçalo, ao Ivan, à Francisca, à Mariana, à Bárbara, ao Tiago, à Liliane, ao Rui, à Anabela, ao Cristiano, ao Tó, ao Diogo (Bolacha), ao Nuno (Rocky), ao Zé, à Mila, à Liseta, ao Tiago Branco, ao Edgar, à Marta, à Ivana, ao outro Tiago, à Xana, ao Castro, ao Lemos, à Vera e ainda a todos os que estão por perto desde há muitos anos pela energia positiva, carinho, amizade e pela festa com quilos de chocolate; tudo para conseguirem tornar estes meses muito mais motivadores e interessantes (e tornaram)! Obrigada também por me acompanharem nas aventuras por um mundo melhor, por partilharem o valor das experiências diferentes, dos conhecimentos transversais e por me bengalarem e relembrarem do que eu era antes disto tudo.

Aqui também tenho de agradecer aos meus pais, não só pelos chocolates, mas acima de tudo por simplesmente confiarem (exatamente como eu gosto) e por proporcionarem tudo o que fosse necessário, acreditando que chegaria facilmente ao fim.

Finalmente, sem dúvida o melhor e maior apoio emocional e incondicional, agradeço ao Pedro. Não existindo agradecimentos suficientes para ele, uma vez que a compreensão para com o meu mundo de mil paixões, o amor, a paciência, a omnipresença e a confiança não têm medidas para agradecimento.

Obrigada!

Sara Francisco

Contents

List of Figures

List of Tables

List of Abbreviations

AFI	Autofluorescence Imaging
AGF	Autocorrelation Gabor Filters
BoW	Bag of Visual Words
CAD	Computer Aided Diagnosis
CCD	Charge Coupled Device
CLE	Confocal Laser Endomicroscopy
CT	Computer Tomography
CV	Computer Vision
DOG	Difference of Gaussians
FICE	Fujinon Intelligent Chromoendoscopy
FN	False Negatives
FP	False Positives
GLCM	Gray Level Co-occurrence Matrix
GLCM	Gray Level Difference Matrix
HME	High Magnification Endoscope
k-NN	k-Nearest Neighbors
LBP	Local Binary Patterns
LTP	Local Ternary Patterns
MRI	Magnetic Resonance Imaging
NBI	Narrow Band Imaging
RF	Random Forest
RGB	Red, Green and Blue
SIFT	Scale Invariant Feature Transform
SUSAN	Smaller Univalue Segments Assimilating Nucleus
SVM	Support Vector Machine
TN	True Negatives
TP	True Positives
WCE	Wireless Capsule Endomicroscopy

Chapter 1

Introduction

1.1 Overview

Prevention is better than cure.
Desiderius Erasmus (1466–1536)

The prevention of all diseases is certainly the best cure, although not always possible. Cancer is a leading cause of death worldwide, justifying the need for its prevention. It is caused by changes in the genetic information of cells, that lead to an uncontrolled division and growth of new ones. Cells lose their predefined function, causing the failure of tissues. In case of malignancy, it can also affect the tissues of other organs, spreading widely through the human body[1].

The difficulty of the forethought of its appearance, the lack of early symptoms and the impossibility of detecting symptoms from cells in the whole body in routine procedures makes the diagnosis a difficult task, stimulating the exponential increase of research in this field. Early detection and possible intervention in the human body can increase the life expectancy in cancer patients.

Cancer in the gastrointestinal track is one of the most common types of cancer (Siegel et al. [50]), with 1.8 million deaths per year worldwide. Technology to detect and treat cancer in its early stage has developed greatly in the last two centuries (Berci and Forde [3]), although 30% of the deaths still occur in the developed countries. In this group of countries, innovative technologies, such as computer systems, made the bridge between the physician and the devices of inspection of the gastrointestinal track, to reduce the subjectiveness of the detection, diagnosis, treatment and monitoring of lesions.

Nowadays, thanks to the technology a physician is able to detect cancer with great accuracy, diagnosing and distinguishing between different stages of the disease. Nevertheless, mortality rate is still too high and the role of prevention is to decrease it. There are some existing limitations, such as the time, the dependence of the image features and the computation complexity of processing medical images, which are the bottom line of this work. Moreover, an inexperienced physician

[1] According to the World Health Organization's Cancer Fact Sheet number 297, February 2011

faces moments of doubts and a wrong diagnosis of cancer must be avoided. Here, the technology and the existing Computer Vision (CV) techniques commonly used in Computer Aided Diagnosis (CAD) Systems for gastroenterology to overcome the limitations faced by the physicians are discussed and a new methodology is proposed and characterized.

1.2 Motivation

In the past few years, CAD systems have established themselves as important tools for physicians daily practice (e.g. in pulmonary (Wormanns et al. [69]) and breast (Jiang et al. [27]) cancer, for the detection of tumor masses). Acting as a reliable second opinion for the diagnosis, these systems are capable of extracting quantitative information from medical images and, thus, guide the physician (Kuo et al. [31]).

Relevant medical fields of research, which is the case of gastroenterology have been using these methodologies with good results. Typical diagnosis systems are based on endoscopic probes, which capture images of the gastroenterological tract. The physician looks for specific patterns in those images and with the help of such systems he can complement his decision about the patients' lesion.

Current CV methodologies encompass devising hand-made features for describing natural or biological images. The success achieved so far is limited however due to the large amount of possible variations that an object can have in an image. In this dissertation, we explore how a system can be designed to analyze gastroenterology images without requiring heavy human interaction.

1.3 Software

All the tests were performed using Mathworks Matlab R2012b and the VLFEAT library [2].

1.4 Objectives

This work aims at understanding the relevance and how engineering tools can be used to detect early on various stages of cancer in the gastrointestinal tract. We intend to explore the characteristics of the medical instrumentation currently in use, as well as understand how adequate both the existing and novel CV solutions for pattern recognition. The main objective of this work is to develop a methodology that processes, describes and classifies endoscopic images with precision. It is supposed to automatically learn the most discriminative patterns which allow to distinguish between different stages of gastric cancer without the intervention of a researcher.

[2] http://www.vlfeat.org

1.5 Contributions

The contributions of this work are listed below:

1. A new methodology using Random Forests (RF) for the recognition of different stages of cancer (normal tissue, dysplasia and metaplasia) in gastroenterology images, improving the accuracy rate exhibited in previous work in the field.

2. The proposed methodology software, available online in http://sarafranciscothesis.pt.vu/;

1.6 Document Structure

This document is organized as follows. In Chapter 2, we start by contextualizing this research, emphasizing its biomedical relevance while giving insight about the physiology of the gastrointestinal system and existing instrumentation for endoscopy; finally, we describe the current CV methodologies used to analyze endoscopy images. In Chapter 3, we fully describe our proposal for endoscopic images analysis and classification methodology. Finally, in Chapter 4 and in 5 the results of the evaluated parameters are discussed and the conclusions of out work presented, respectively.

Chapter 2

Cancer in the Gastrointestinal track and Technologies

Cancer on the gastrointestinal tract is one of the most severe cancers, due to its high mortality rate and prevalence. Its detection, similarly to what happens with the other types of cancer, is no longer a strictly medical task. Indeed, it combines the medical know-how with relevant advances in oncology and novel and innovative techniques for an objective characterization of tissues, the latter provided and developed by biomedical engineers.

The relationship between medicine and engineering has become closer over the past few years, allowing the physicians to evolve from simple semiology (analysis of naked-eye signs and symptoms) to the usage of tools which provide an objective and reliable evaluation of the patient, (for example, endoscopes or, more recently, computer-aided diagnosis systems). These solutions, although innovative, are still not versatile enough to be able to address unknown or unseen variations of the morphology of tumors, as well as the eyes of experienced physicians can. This handicap is also extended to inexperienced physicians, motivating the development of a gastroenterology image analysis system that embeds cancer recognition strategies, allowing a future training or examination to have a reliable evaluation of new and challenging cases.

In this Chapter the context of our work is presented, providing a transversal understanding of the whole gastroenterological cancer detection problem. We start by exploring the characteristics of the cancer of the gastrointestinal tract, the importance of its study, followed by the instrumentation technology for cancer detection. Finally, the methodology proposed in this work, as well as the CV methodologies used for gastroenterology images analysis in which it is based on are introduced.

2.1 Overview

Gastrointestinal cancer occurs in the organs of the digestive system, which includes the esophagus, stomach, gallbladder, liver, pancreas, stomach, small intestine, colon and rectum. Each of these organs has a unique shape and is composed of a type of tissue exposed to different conditions,

making the cancer detection procedures difficulty and requiring them to be individually adapted (Seeley et al. [47]). Nevertheless, all cancers can be caused by eating habits, derive from other pathologies or some hereditary conditions. There are five stages of the disease (grades from 0 to IV), enforcing the need for early treatments (Jankowski and Hawk [25]).

In this section, the importance of cancer detection, the physiology of the organs on the gastrointestinal tract, the limitations of the available detection devices and technology will be studied. The main goal is to draw conclusions about the current detection and diagnosis technology and the research fields in which improvements are required.

Morphology and Physiology

Figure 2.1a depicts the gastrointestinal tract, emphasizing the organs of the digestive system relevant for this work, since these organs allow an acquisition of images. These organs have a similar histology, although playing distinct roles in the digestive process. There are four main cellular layers: the inner mucosa, the submucosa, the muscular layer and the external serosa, Figure 2.1b (Seeley et al. [47]).

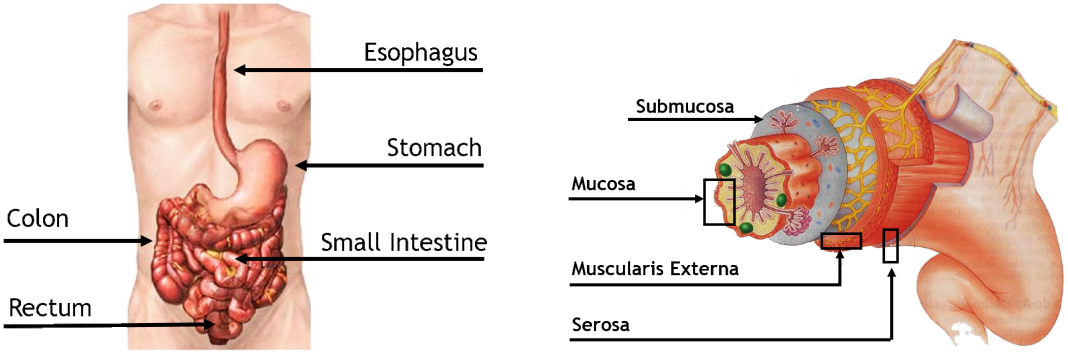

(a) The gastric canal.

(b) Histology of the gastroenterologic tract.

Figure 2.1: In (a), the anatomical location of the gastrointestinal tract is shown. The typical histology of tissues on the gastrointestinal tract is presented in (b). Adapted from Seeley et al. [47].

There are three main types of cancer in the gastrointestinal tract: metaplasia, dysplasia and neoplasia (Kapadia [28]). The first one consists simply in the differentiation from a healthy cell to its abnormal or mutated version. On the other hand, dysplasia, although still a reversible process, promotes a disordered growth and maturation of tissues. Neoplasia is an irreversible change of cells. The grade associated to a certain cancer depends on the location of the tumor and its specific histology. The stage 0 of the gastrointestinal cancers is called dysplasia. The tumor invades or is generated in the mucosa of an organ. The following stages require the spreading through the inner layers of a tissue. The most severe stage (IV) happens when the tumor spreads systemically and

metastasis are found in other organs (Jankowski and Hawk [25]).

Statistics and Mortality

Currently, more than 14 million people per year are victims of cancer worldwide. 2,1 million of them present pathologies on the colorectum, esophagus or stomach (see Figure 2.2a). There are around 1,8 million deaths every year, 30% in the more developed countries, where more advanced technology and diagnostic procedures are used (Ferlay et al. [13]).

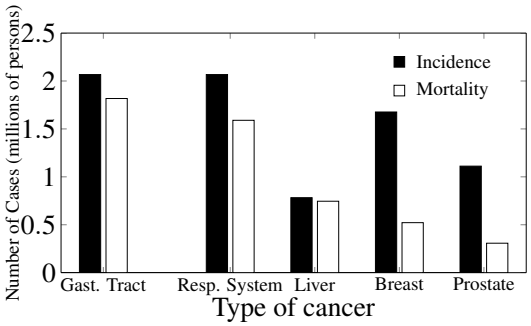

(a) Cancer incidence and death rates in 2014, by type of cancer.

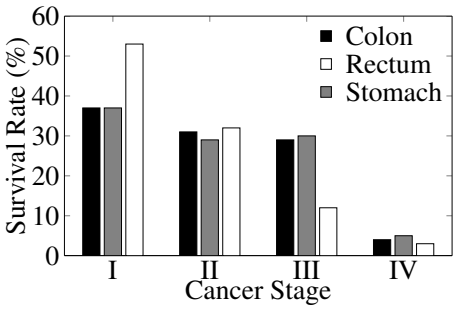

(b) Survival rate by type of cancer on stomach, rectum and colon.

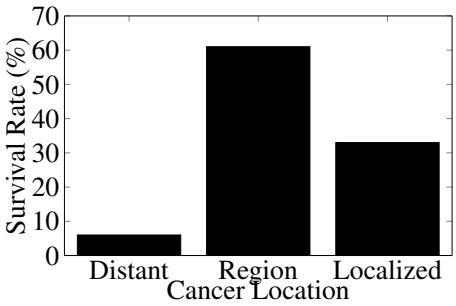

(c) Survival rate with respect to location of esophagus cancer.

Figure 2.2: Relevant statistics about the incidence and mortality of cancer on the gastrointestinal tract, and its relationship with other types of cancer.

Figure 2.2b and Figure 2.2c present the survival rates of cancer of the gastrointestinal tract[1].

[1] Adapted from: http://www.cancer.org/index

As can be observed, the survival rate increases with the early cancer detection (Areia et al. [2]). The analysis of images in the gastrointestinal tract allows the visualization of structures and plays a major role in the early detection of the pathology. From this, and based on the aforementioned statistics, it is mandatory to improve the cancer detection procedures and the existing technology.

Diagnosis and Detection

The common techniques used to diagnose gastrointestinal cancer are briefly present in Table 2.1. Cancer detection has a complex nature and may involve different medical routines, from general exams to high-resolution medical imaging procedures.

Table 2.1: Techniques used for gastrointestinal cancer detection (Yuan [72] and Lee et al. [32]).

General exam of the body	Performed by a general practitioner, in which systemic signs of the disease are searched for. The patient history and its health habits are discussed and evaluated. Patients with problems on the structures of the gastrointestinal tract are directed to a gastroenterologist.
X-Ray	The most common and non-invasive medical imaging routine. In it the organs are observed. From a two view acquisition, it is possible to infer if abnormal masses are present in the abdominal cavity. However, X-ray is not enough for an early detection.
Endoscopy	An endoscope passes down the throat of the patient. Endoscopes are thin, flexible, camera-holding and illuminated tubes. They allow the observation of the esophagus, stomach and the first section of the small intestine. Potential abnormal areas are searched for and biopsies (tissue samples) can be collected for further laboratory analysis. There is a myriad of endoscope configurations possible. It is the most used technique to diagnose cancer on the gastrointestinal tract.
Virtual Endoscopy	*Magnetic Resonance Imaging (MRI) and Computer Tomography (CT):* High-resolution medical imaging techniques, only used when the other diagnostic procedures fail. They can provide with high certainty the location of the abnormal masses and are usually essential to direct the treatment based on the location of the tumor. Provide relevant information for surgical procedures.

The early detection of the disease demands the observation and histological examination of the abnormal cells. Therefore, the endoscopy is nowadays the most used procedure for these cases.

In its early years, 1860s, endoscopy found two physical limitations: the gastrointestinal tract is not straight and there is no light inside the body (Sivak [54]). Some years after the invention of the light bulb, a mirror and light system was developed, eliminating the problem of the darkness.

However, only in the 1960s was the flexibility of the device achieved. It was then possible to use an eye piece and optic fiber, strategically organized to transmit not just light, but also to acquire images. This is the true ancestor of the device used nowadays, the flexible endoscope. Modern endoscopes are very compact devices, including a Charge Coupled Device (CCD) for acquiring images or film and a light source on the distal tip (see Table 2.2). Endoscopes are also equipped with an accessory channel, allowing the entrance of medical instruments to collect tissue samples in a minimal invasive procedure (Berci and Forde [3] and Liedlgruber and Uhl [34]).

Table 2.2: Main achievements in Endoscopy (Berci and Forde [3]).

Year	**Achievement**
1868	First Gastroscopy, credited to Kaussmaul
1961	First device with articulated lenses and prisms
1920	Flexible quartz fibers first concept
1954	First flexible endoscope model
1969	Invention of CCD

Clinical literature states that the usage of endoscopes provides high early detection rates and leads to a good prognosis, thus preventing the cancer from evolving into more dangerous stages. Since medical endoscopy is a minimally invasive and relatively painless procedure, allowing us to inspect the inner cavities of the human body, endoscopes play an important role in modern medicine. However, an accurate cancer detection and diagnosis is still difficult. This is mostly due to the lack of visual cues that suggest the presence of cancer in its early stages (Singh et al. [52]).

Complementing endoscopy with biopsy allowed physicians to collect direct histological information from the organ being analyzed (Yuan [72]) and the technological advancements in endoscopy digital tools improved the cancer recognition rate, when compared to ancestor techniques (Lee et al. [32]).

Both the design of endoscopes and the ability to take digital pictures motivated the usage of CAD support systems for gastrointestinal images. These are intended to help the diagnosis, acting as a first or complementary opinion to physicians in general applications. Specifically on the gastroenterology domain, the implementation of common CV tools has made it possible to detect and describe quantitatively the visual features leading to an useful automated decision (Liedlgruber and Uhl [34]). Such could be achieved using MRI or CT-scans but, although reliable, such diagnostic methods are computationally complex, costly and require users to be highly familiar with technology (Liedlgruber and Uhl [34]). This created the need for a simple, practical and affordable tool, developed for a *user-shaped* evaluation of gastrointestinal images, capable of being implemented on a daily routine practice.

2.1.1 Endoscopes

An endoscope is a medical device capable of acquiring both images and even tissue samples from the gastrointestinal tract. Although a lot of configurations are possible, all endoscopes share some

characteristics: (a) they are composed of a flexible tube; (b) illumination and image acquisition tools are incorporated; (c) this device has an accessory channel where some claws can be added, especially for biopsy samples capture. Different endoscopy techniques are described below.

Standard and High Definition Endoscope: The standard definition endoscope is equipped with a CCD chip, acquiring an image signal with 100-400 pixels and images with a defined aspect ratio of 4:3. The High-definition endoscope has a similar configuration but provides images of higher resolutions. Consequently, the physician can detect subtle changes in the mucosa more easily. Its images have a resolution 10 times higher, two different images aspect ratio and its monitors can display progressive images while in progress. The frame rate of 60 times per second decreases the amount of noise and allows the accurate capture of fast motions (Subramanian and Ragunath [60]). See Figure 2.3a.

High Magnification Endoscope (HME): The technological advances have lead to the development of the HME. It has electronically movable lenses which allow real time visualization of mucosa morphology in greater detail (Singh et al. [53]). The endoscopic image is zoomed up to 150-fold, while keeping high detail and resolution. This is a major improvement when compared to common digital zoom or electronic magnification systems. In HME, the image is moved closer to the display, decreasing the number of observable and the image resolution. Most conventional endoscopes are capable of electronic magnification of 1.5-fold to 2-fold but require a compatible processor.

These endoscopes were widely studied by Stevens et al. [59], in a work that looked at the early diagnosis of cancer in the gastrointestinal tract, especially metaplasia and dysplasia. Although this technique is easily available with high resolution, it was designed to increase the visualization quality and lacks a diagnose-oriented framework. See Figure 2.3b.

Autofluorescence Imaging (AFI): Recent endoscopes use autofluorescence imaging (AFI). AFI detects the natural fluorescence of tissues, which is emitted by specific light-excitable molecules. It is possible to capture color differences in the fluorescence emission in real time, because of their unique fluorescence spectra. This technique allows tissue characterization and can be used to detect a significant number of patients with high grade early cancer (Singh et al. [53]). See Figure 2.3c.

Chromoendoscope: This technique is based on the enhancement of the surface of the mucosa by applying different dyes. Depending on the followed protocol, different stains are used, thus making different anatomical structures more prone to be observed. Obviously, there are endoscopes with different sensibility for each dye (Rácz and Tóth [43]). There are two essential stages in chromoendoscopy: (1) removal of mucous, normally using water; and (2) dye application. A more detailed overview on this technique is available on (Singh et al. [53]). See Figure 2.3d.

Virtual Chromoendoscopes: Virtual Chromoendoscopy is nowadays the most widely used technique in endoscopy. Being a reliable alternative to the time-consuming chemical chromoendoscopy, it allows the enhancement of the mucosal surface without applying color dyes. A better contrast of the vascular patterns on the mucosa is often achieved recurring to Computer Vision techniques.

- **Narrow Band Imaging (NBI):** The need for a simpler endoscopy technique led to the development of the NBI, firstly described in Ohyama et al. [39]. The common endoscopes illuminate the scene of interest using white light, which results from the fusion of three light waves: green, blue and red. NBI narrows the bandwidths of blue (440-460 nm) and green (540-560 nm) wave light, while the contribution of the red wave light is totally discarded from the emitted light (Singh et al. [53]). The main advantage of narrowing the green and blue light spectra is an enhancement of the microvasculature pattern (due to a superficial penetration of the mucosa and to an absorption peak of hemoglobin for these wavelengths). Images obtained using NBI endoscopes were tested with promising results in Curvers et al. [10], Mannath et al. [36]. See Figure 2.3e.

- **i-scan:** This technique consists of three types of algorithms: Surface Enhancement, Contrast Enhancement and Tone Enhancement. Surface Enhancement enhances the light-dark contrast on the image, by obtaining the luminance intensity data for each pixel. Then, algorithms for the detailed observation of the mucosal surface structure are applied. Contrast Enhancement digitally adds blue color in relatively dark areas: the luminance intensity data for each pixel is obtained and subtle irregularities around the surface are computationally enhanced. Both enhancement functions work in real time without impairing the original color of the organ. Additionally, both are suitable for screening endoscopy to detect gastrointestinal tumors at an early stage. Finally, Tone Enhancement dissects and analyzes the individual RGB components of a normal image. Then, the color spectrum of each component is altered and recombined with the other components into a single, new color image. This approach was designed to enhance mucosal structures and subtle changes in color. The i-scan technology leads us to easier detection, diagnosis and treatment of gastrointestinal diseases (Kodashima and Fujishiro [30]).

- **Fujinon Intelligent Chromoendoscopy (FICE):** FICE can simulate an infinite number of wavelengths in real time. The system has 10 channels that are designed to explore the entire mucosal surface. Each channel corresponds to the three specific RGB wavelength filters, but there is no setting specifically used for a given gastroduodenal condition (Coriat et al. [7]). See Figure 2.3f.

Confocal Laser Endomicroscopy (CLE): CLE provides high-resolution microscopic images at sub cellular resolution, streaming the deepest layers of the gastrointestinal mucosa. The term confocal refers to the alignment of both the illumination and collection systems in the same focal

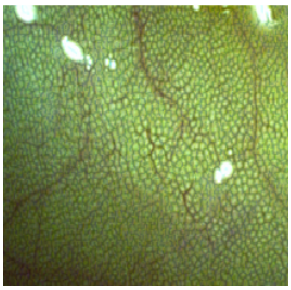

(a) High Definition Endoscope image

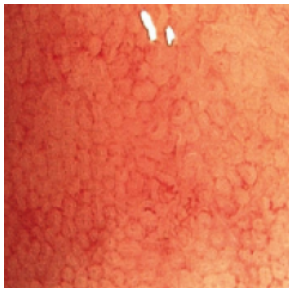

(b) High Magnification Endoscope image

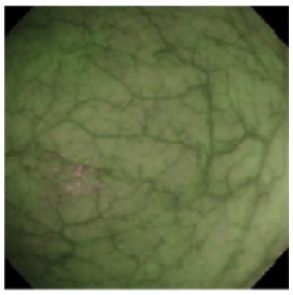

(c) Autofluorescence image

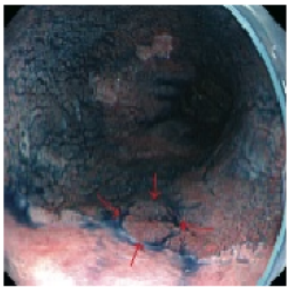

(d) Chromoendoscopy image

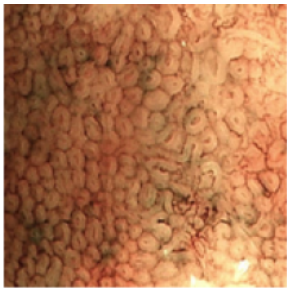

(e) NBI and High Definition Endoscope image

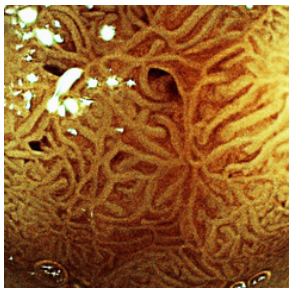

(f) Fujinon Intelligent Chromoendoscopy Image

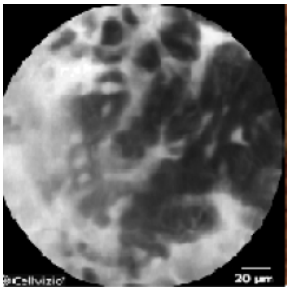

(g) CLE image

Figure 2.3: Representative images of seven endoscopy technologies: **(a)** High-resolution endoscopic image of the surface of normal mucosa. **(b)** HME of normal intestinal mucosa and the same image on **(e)**, seen with NBI and HME (Haidry and Lovat [21]). **(c)** AFI in the normal colon (Fujiya et al. [16]). **(d)** Indigo carmine (the dye) chromoendoscopy of a mucosal lesion detected in a patient with Barrett's esophagus (Haidry and Lovat [21]).**(f)** Mucosal capillary and surface pattern were detected with FICE with magnification (Yoshida et al. [71]). **(g)** Images of normal tissue using probe based CLE ([21]).

plane. Laser light is focused through a pinhole at the selected depth via the same lens (Liedlgruber and Uhl [34]). See Figure 2.3g.

Unfortunately, the visual criteria for malignancy is still under clinical evaluation, as stated in Shui-Yi Tung et al. [49], thus making it impossible for the scientific community to evaluate the potential of this new technique. Additionally, such a complex methodology requires experienced users to correctly manipulate it and thus achieve good results.

Wireless Capsule Endomicroscopy (WCE): The inspection of the small intestine is a difficult task due to its long and convoluted shape. WCE was designed to overcome this limitation and to make endoscopic procedures safer, less invasive, and more comfortable for the patient.

In this case, the endoscope is not a flexible tube but a capsule that the patient swallows. The small capsule is equipped with a light source, lens, camera, radio transmitter, and batteries. Propelled by peristalsis, the capsule travels through the digestive system for about eight hours and automatically takes more than 50 000 images. These are transmitted via wireless to a recorder worn outside the body (Liedlgruber and Uhl [34]). Currently, WCE seeks not only to inspect the small intestine, but other organs such as the colon or the esophagus. The main drawbacks of WCE consist in the lack of ability to obtain biopsy samples, contrary to other endoscopy techniques.

Table 2.3 presents a summary of the main applications of the technologies previously described and currently commercialized (Subramanian and Ragunath [60]). Although recent solutions are accurate and equipped with recent technology, thus the best solution adapted for each case that implies a combination of more than one technique, the perfect endoscope is still to be developed. (Song and Wilson [56]).

Table 2.3: Summary of the current endoscopy techniques used applications (Liedlgruber and Uhl [34]).

Endoscope	Application	Target Tissue
Standard and HD	Used combined with other technologies like die-based and Virtual Chromoendoscopy	Surface enhancement. Reduce Artifacts.
High Magnification	Identification of neoplasia	Surface/vascular detail.
AFI	Identification or early detection of neoplasia	Displasia
NBI	Identification of neoplasia specially combined with Magnification Endoscopy.	Vascular Contrast of capillaries and submucosa enhancement
I-scan and FICE	Identification of neoplasia specially combined with Magnification Endoscopy.	Structural and vascular enhancement
CLE	Identification of neoplasia	Subcelular structures

Conclusion: The endoscopic devices presented previously allow the physicians to inspect all the inner cavities of the alimentary canal, even the intestine, thanks to the capsule endoscopy. Although the differences in the resolution of the images acquired by different devices, the differ-

ences between the acquired images by these devices are not the main limitation for the accuracy of current CV techniques. The major constraint is in the existent methodologies which are still not able to extract the most descriptive features or describe better the information contained in the medical images. This constraints and the attempts to overcome this in the gastroenterology field are presented in the next Section.

2.2 Computer Vision in Gastroenterology

The acquisition of images of the gastroenterological tract using endoscopic probes is a procedure prone to noise. As it is performed in non-controlled conditions, some problems regarding illumination, rotation, shadows or occlusion occur. CV in gastroenterology has to deal with these vicissitudes and also with very feeble visual patterns which hampers the lesion recognition capability.

The previously developed works in this field of research comprised a wide variety of standard CV techniques. Nevertheless, they are still limited in some of the aforementioned acquisition constraints or the resultant classifier is just optimized to a range of images, instead of being robust to any dataset. In this field it would be valuable the use of an algorithm able to robustly extract the relevant features, thus allowing its application in any gastroenterology images.

Although we are trying to answer to a medical problem, it is also a pattern recognition challenge. A possible solution may include other image processing algorithms that have not been tried before in this field.

Figure 2.4 shows a common pipeline for the acquisition and processing of endoscopic images in a CAD system. This document has previously presented endoscopic image acquisition devices and in this section we detail the procedure for the processing and recognition of cancer in gastroenterology endoscopic imaging. In particular, we give special emphasis to the Feature Extraction and Image Description in order to introduce our proposal, since they are the most challenging stages and the scientific community looks forward to guarantee better accuracies. After, we introduce the strengths and limitations of the state of the art methodologies, as well as a methodology designed by us to overcome such weaknesses, proposed in Section 3.

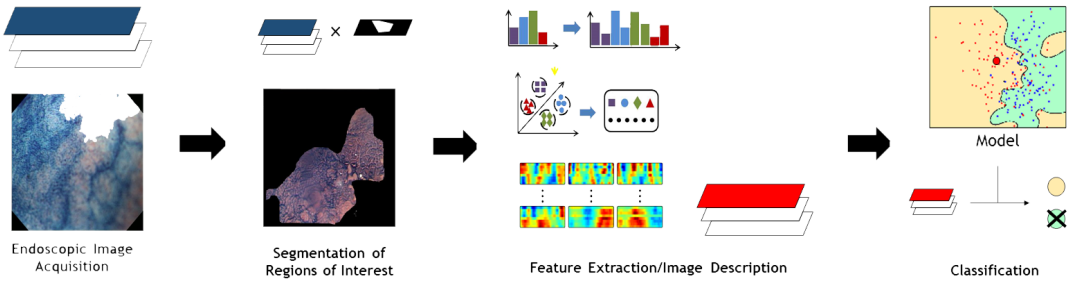

Figure 2.4: Overview of the pipeline of acquisition and processing of endoscopic images by a CAD systems, focusing the image description stag, which is the main focus of this work.

2.2.1 Image Processing

Feature analysis intends to gather information from images. A feature is a point or image region that is salient, relevant and distinctive from its neighbors (Zitova and Flusser [73]). The ideal type of features must be invariant to noise, which can be caused by undesired motion of endoscopic probes, shadows or occlusions. A good feature presents at least the following characteristics:

- **Repeatability**: which is achieved when different images of the same gastrointestinal lesion show corresponding feature points;
- **Distinctiveness**: obtained when a certain feature is specific for a certain lesion;
- **Accuracy**: features must be located exactly where distinct points of the lesion are found (Tuytelaars and Mikolajczyk [65]).

This canonical definition was firstly applied to static scenes or objects, relying on the detection of corners (as Harris in Harris and Stephens [23] or Smallest Univalue Segment Assimilating Nucleus (SUSAN) corner detectors in Smith and Brady [55]), edges or high-level features. These latter ones are already associated to image description and representation. In the gastroenterology field, high-level features have been used in studies with different purposes: detection of gastric ulcers (Kodama et al. [29]), to make a generic description of the intensity values and detect intensities changes along different regions of the images (Häfner et al. [20]) and differentiate between cell-types in colorectal polyps (Gross et al. [18]). They present some pleasing results for standard scenes, but not flexible and accurate enough to deal with the acquisition problems and to guarantee the extracted features are relevant enough for a powerful description. Due to this, standard methods, such as corner and edge detectors, have been discarded since and are absent from recent works in this field.

Along with simple detectors and high-level feature extraction methodologies, other approaches were developed. Region detectors, which often enhance homogeneous regions in images, were one of those. A region is an image area that has an averaging intensity distinct from that of the surrounding neighbors, defined by applying custom-made segmentation algorithms. These regions are expected to be descriptive of the image content and class that is being searched for. Although important, this is not the focus of this thesis, since we aim at describing the regions of interest in gastroenterology images, not detecting such regions. In fact, our dataset consists in previously segmented images by experienced physicians.

Frequency Domain Features

Frequency Domain features are a decomposition of the image information of the spatial domain into frequency domain, obtained by Fourier transformations. In the Fourier domain, each point represents a particular frequency contained in the spatial domain image. From the new spectrum of features that Fourier transformations gives, it is possible to describe the image from a different perspective (Liedlgruber and Uhl [34]). In Haefner et al. [19], the authors explore the

application of Fourier filters to distinguish between six types of mucosal texture and *pit-patterns*, each one with specific spatial distribution and response to the filters. Fourier transformations were also used by Vécsei et al. [67], applying its highly discriminative power to the classification of duodenal images. The authors mapped the images on the Fourier Space using a bank of filters and selected the most discriminative features for each RGB color channel using an Evolutionary Algorithm. As a whole, Fourier transformations can be used to obtain the power spectrum of an image, compute statistical features and use them for classification, as described by Liedlgruber and Uhl [34].

Wavelets also allow the mapping of images into the frequency domain. They are described as a mathematical tool, useful to extract specific information from images by the parametrization and customization of the wavelet. Its analysis provides information similar to what occurs in the human visual system, performing a hierarchical edge detection at multiple levels of resolution (Liedlgruber and Uhl [34]).

From the different types of wavelets that can be applied to image processing methods, Gabor Filters take the lead in the gastroenterology field (Riaz et al. [44]). Autocorrelation Gabor filters (AGF) were firstly presented by Gabor [17]. They are based in the principles of a simple cell in the mammalian visual cortex. These cells are characterized by their band pass nature and direction selectivity, making them respond only to specific spatial frequencies and orientations. The filtering stage guarantees their invariance to illumination, rotation, scale and translation. This is because, although the image can be rotated or translated, the frequency content of the image remains the same, thus making them always detectable (Riaz et al. [44]). According to Riaz et al. [44], AGF is capable of performing a feature detection stage together with the computation of image descriptors, while being invariant to rotation and illumination changes. Then these descriptors are used by a previously trained classifier to obtain a suggestion of the diagnosis.

Although new approaches, such as the one presented in this thesis, explore the application of other machine learning methodologies to the analysis of gastroenterology images, frequency domain features remain a strong research field in this topic, since they mimic the sensing capabilities of the human visual system. It is believed that following this premise, we can be able to extract more and better information about the patterns in an image.

Spatial Domain Features

Spatial Domain Features consider texture and pixel-based information, by building histograms and computing statistical parameters from the extracted data. In fact, the standard methodologies for the classification of gastroenterology images often rely on texture analysis techniques (Liedlgruber and Uhl [34]) and correlate changes with the intensity with their location in the images.

One of the most well known methodologies for texture analysis is the LBP (Local Binary Patterns)(Ojala et al. [40]). This methodology searches for uniform patterns computed over an image, whose occurrence is counted into an histogram, effectively estimating the distribution of microstructures (edges, lines, regions). The detection of these structural features allows to describe

the images. This quantization of feature distribution can be performed by combining multiple operator for multiresolution analysis: different search radius and angles. This analysis is centered on the image intensities inside a small processing window (often *(*3x3)), that are binary labeled (0 or 1) with respect to the average intensity inside the neighborhood in which they are contained. This processing enhances the aforementioned structures, believed to provide a good detection of pattern changes between different images or image regions.

LBP is popular in texture analysis because of its rotation invariance. Also, the intensity differences are not affected by minor changes in the mean luminance of images, since the intensity values are not highly compromised. In other words, the binary pattern of the region only changes if the gray-scale intensity of, at least, one pixel becomes higher or lower than the mean intensity in that neighborhood. So, if no relevant changes in the gray-scale values are found, the region keeps being defined by the same binary pattern.

An improvement was described by Tan and Triggs [61] where the LTP (Local Ternary Patterns) were presented. This descriptor, in opposition to LBP (which describes a texture using a binary pattern, 0 or 1), calculates the texture of a Region of Interest computing a pattern of three values. Using ternary patterns instead of binary patterns increases the resolution of the descriptor. More recently, in Hegenbart et al. [24], authors have started by presenting a wide study about the state of the art methodologies for duodenal lesion classification using computer vision techniques. They show that an affine-invariant version of the LTP can be used for the description of duodenal images with good results. However, this methodologies are not immune to luminance and scale variations, which interfere in the intensity value on the image.

GLCM (Gray Level Co-occurrence Matrix) is another typically used methodology in gastroenterology (Dhanalakshmi et al. [11]). Proposed by Haralick et al. [22], it is a matrix that counts all the transitions between the intensities of an image region, in a specified direction and radius. Each specific texture is defined by a set of transitions with associated probabilities, where measures such as the contrast, energy, homogeneity, and entropy can be obtained. Although similar images allow us to obtain similar GLCM, it is also true that completely different patterns with similar intensities can lead to GLCM that are alike (Haralick et al. [22]).

In the subsequent years, some modifications to GLCM were introduced. One of them is GLDM (Global Level Differences Matrix), which computes differences between the pixels on the region of interest rather than counting intensity transitions. In Onji et al. [41] the capability of these texture descriptors, especially to describe endoscopy images is studied. As these methods are highly dependent on the pixel intensities, the output can be compromised by luminance changes over time. In other words, as the endoscopic image acquisition is performed in a non-controlled environment, the texture analysis will answer to every intensity variation, even if it is artificial or caused by other artifacts. Thus, GLCM or GLDM may not provide the most robust solution.

In the same work, the authors show that the SIFT (Scale Invariant Feature Transform) descriptor performs a better quantitative description than the GLDM for the same dataset. The SIFT (Lowe [35]) descriptor extracts keypoints based on image texture. A SIFT keypoint is a blob-like,

circular image region with a specific orientation. It is described by the following geometric parameters: the keypoint center coordinates, its scale (the radius of the region), and its orientation (an angle)[2].

Then, taking into account the selected keypoints, SIFT computes a 128-feature space descriptor, invariant to translation, rotation and scale, also minimally influenced by noise and illumination. To achieve this, SIFT searches for keypoints at various scales and positions, following the basic strategy of the DoG (Difference of Gaussians) method (Crowley and Parker [8]). The main advantage of SIFT is that, not only allows a robust localization of relevant features, but also computes descriptive information.

Embedding Local Features in Global Image Description

The canonical separation between global and local feature extraction strategies is related to choosing whether we want to describe image properties as a whole (global features) or to extract relevant information from each of the sub-regions of the images (local features). Local features provide an intuitively better description, since they are not affected by noise in distant regions of the images, are less prone to lose fine changes in the texture of images and distinguish better between foreground and background (Tuytelaars and Mikolajczyk [65]). Their better descriptive power is also due to their distinctive representation of relevant regions of the image, while remaining invariant to viewpoints and illumination changes (Trzcinski et al. [64]).

However, powerful local descriptions require a very subtle tuning of parameters, otherwise the extracted information lacks context and we miss important information about the images. Moreover, Tuytelaars and Mikolajczyk [65] state that, unlike what it is expected, global descriptors work well for images with distinctive colors and at least, with homogeneous or characteristic texture. In gastroenterology images, texture homogeneity is almost impossible to achieve, thus making global descriptors a weak option, despite the obvious need for context. Although the image description using local features and global features may seem unlikely to achieve, their fusion into a single powerful description strategy would overcome these individual weaknesses and provide a more reliable tool for feature extraction.

Following Chatfield et al. [6], this study explores the potentialities of visual bagging. Briefly, we intend to extract local features to improve the discriminative power and overcome possible acquisition constraints, then combining it into a Bag of Visual Words, that globally describes the image using the local extracted features. This mapping contextualizes the extracted information and is expected to guarantee a more fine and detailed characterization.

2.2.2 Machine Learning

In the gastroenterology field, the vast majority of studies have been using SVM (Support Vector Machines) (Vapnik and Vapnik [66]) and k-NN for classification (k-Nearest Neighbors), due to its importance and versatility in pattern recognition [34]. Although the competitive accuracy rates and

[2] http://www.vlfeat.org/api/sift.html

computational simplicity of k-NN, a supervised classification method that labels an instance based on the closest samples on the feature space, SVM is the state-of-the-art classification method. Details about SVM methodology can be found in Chapter 3.

Among the most common usages of SVM in this field of research are precise tumor detection (Li and Meng [33]) and colorectal polyps classification (Tischendorf et al. [63]). Conversely, k-NN has been applied in a prominent recent work, to find abnormalities in the inner cavities of the gastrointestinal system (Nawarathna et al. [38]).

2.2.3 Open Issues

The methods presented in the previous sections are the most commonly used solutions in gastroenterology. However, in this thesis, we propose an alternative solution for the problem in hands, based on recent works in different computer vision applications. They have given some insight into how to solve the problems related to the classification of cluttered images, with occluded regions of interest and the typical rotation, multiresolution and illumination variations. The proposed solutions, that quantify the number of times each different pattern (visual word) occurs in the images (vocabulary), are expected to be translated to the evaluation gastroenterology images. The set of visual words is know, in CV, as Bag of Words (BoW). More details about BoW generation can be found in the next chapter.

As BoW requires randomness for a representative description, the first strategies were designed using k-means (Csurka et al. [9]), since the centroid locations are randomly defined at the start of each repetition of the algorithm. However, these locations are not linked to the input data, diminishing the correlation of the Bag of Words to the true characteristics of the images. To overcome this, a RF-based framework was proposed by Shotton et al. [48]. The proposed method guides the creation of randomized classification trees using the information on the input images, each node of each tree being a splitting instance that tries to separate, even slightly, different patterns. This way, image regions with varying information are grouped separately, while maintaining the required randomness (Yao et al. [70]), and allowing the computation of quantitative information via histograms. Those histograms can provide distinctive information between images with different classes (more detailed information in Chapter 3). The method proposed by Shotton et al. [48], along with the preliminary study presented by Moosmann et al. [37], although presenting good performances, lack data ranking, i.e. they only use the leaf nodes of each tree on the RF and assume that the branching capabilities of a decision capture all the differences between the patterns on the leaf nodes. However, small changes can provide relevant information that is not included in the analysis when only the terminal nodes are considered. We look forward to evaluate the importance of the information on the splitting nodes, along with that on the terminal ones.

A preliminary attempt to characterize gastroenterology images using BoW has been proposed by Sousa et al. [58], which implements a BoW generation stage using K-means after image description using dense SIFT. The obtained results were promising and motivate the usage of RF to generate a more reliable BoW of the data.

These achievements can provide solutions to overcome the limitations on the classification of endoscopic images using CAD systems. It is expected that a robust BoW can be created from extracting the most discriminative local information on sub-regions of the images and combining them into a single global descriptor. By doing this, we overcome the lack of resolution of a global description, by centering the analysis into specific regions that enclose highly discriminative feature points. Low-level patterns and variations, i.e. more detailed information, is obtained, with the plus that noisy data is likely to be discarded. This way, only relevant information is kept and used for classification.

Chapter 3

Random Forests for Visual Representation in Gastroenterology Examinations

In this Chapter we present the main contribution of this thesis, describing a new methodology for cancer recognition in gastroenterology images. The majority of CAD systems rely on machine learning techniques that fit a classification model to features extracted from the images being analyzed. It is common that features are not powerful enough to distinguish between different classes. Even images descriptors computed after the extraction of these features lack on the capacity of identifying the most discriminative patterns. To overcome this, several methods have been proposed. One efficient way of handling this pattern recognition challenge is to define visual words (textons) and quantify its frequency on the input data. In CV, the ensemble of visual words is called BoW.

Considering a text categorization challenge, the occurrences of each word can be counted to build a global histogram, summarizing the document content in respect to each word frequency (Moosmann et al. [37]). This parallelism explains the usability and the potential of this method for our work. We survey and list all the patterns on an image into a visual codebook and count the amount of times that each pattern appears on the image being classified. Such counting procedure can be perceived as a histogram of occurrences in which image content is summarized and described with simplicity, thus making the construction of an effective classifier easier. This approach has been used to describe common scenes and detect well-defined objects by Shotton et al. [48] with promissory results.

We use RF to generate this BoW, which is a novelty in gastroenterology images classification. RF carry descriptive power and establish an hierarchy over the input data, separating it into patterns in a way that is expected to capture the richness and the diversity of patterns in an image.

The RF is generated by constructing decision trees, which allow the ranking of the data throw the criterion defined by each node of the trees. In each of the nodes of a tree the separation of the different patterns is expected. Although building the decision tree as a classifier, because of its na-

ture, this scheme gives relevant information for pattern recognition, since it is possible to describe the images throw this information. In order to increase the strength of this approach we generate an ensemble of trees, here called forest. Furthermore, each tree is generated independently with randomized attribute choices and threshold definitions, meaning that RF allow a hierarchical clustering that occurs in an unique way in each tree, but always anchored to the intrinsic nature of the input data.

This approach is embedded in a larger processing pipeline, shown in Figure 3.1, which aims at analyzing and classifying endoscopic images dealing with the aforementioned acquisition constraints. Our approach automatically renders representative features from the images, dismissing the need for a specialist to guide its extraction.

The method presented here is an advance in the classification of gastroenterology images because it can accurately distinguish between different classes without requiring previous knowledge about features. In our specific application we are dealing with a multiclass problem, in which the differences between the classes are not evident and we expect to require a robust and highly descriptive method to extract relevant information from the images.

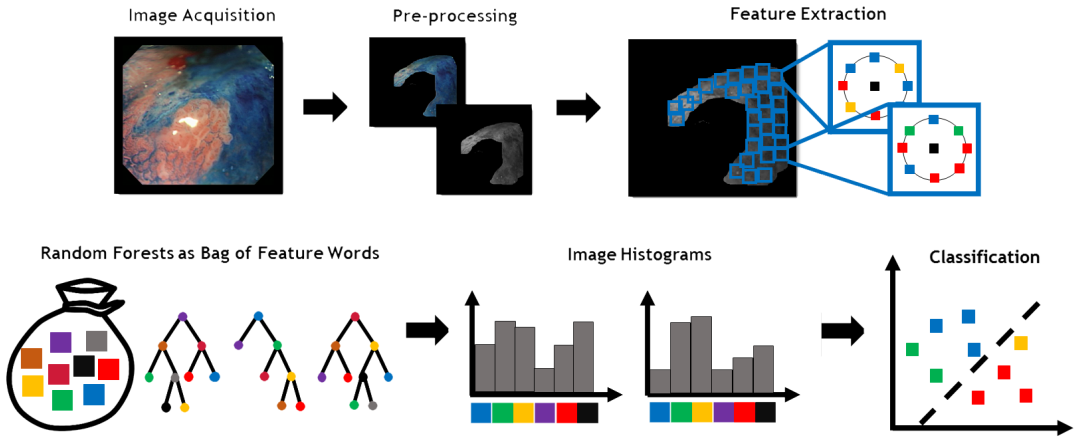

Figure 3.1: Overview of the pipeline of our methodology to build a classifier model for gastroenterology images. The major contributions of our work are related with the BoW and vocabulary construction.

The methodology presented herein comprises the following stages: **(a)** image acquisition; **(b)** image processing for denoising purposes; **(c)** feature extraction stage, in which the images are sampled into patches - arrays with intensities of the pixels of a certain region; **(d)** generation of a Bag of Words from the extracted image information, using Random Forests; **(e)** building the Vocabulary using the generated words to describe all the images; **(f)** train a SVM classifier using the descriptive information from the Vocabulary to predict the class of new images.

In the following Sections we start by providing a theoretical contextualization about Decision Trees and RF and then describe the processing stages of our algorithm, including Vocabulary generation and classification.

3.1 Decision Trees and Random Forests

Decision trees are statistical approaches designed for decision support strategies, because they are self-explanatory, handle both numeric and nominal input attributes and deal well with possible errors or missing values on the dataset (Rokach [46]). They take the input data and subject it to a sequence of binary decisions. This sequence can be seen as an iterative creation of a tree, which branches left or right at each node, or decision point. In other words, the input data follows a specific path while it descends the tree and until it reaches a leaf node, as shown in Figure 3.2a.

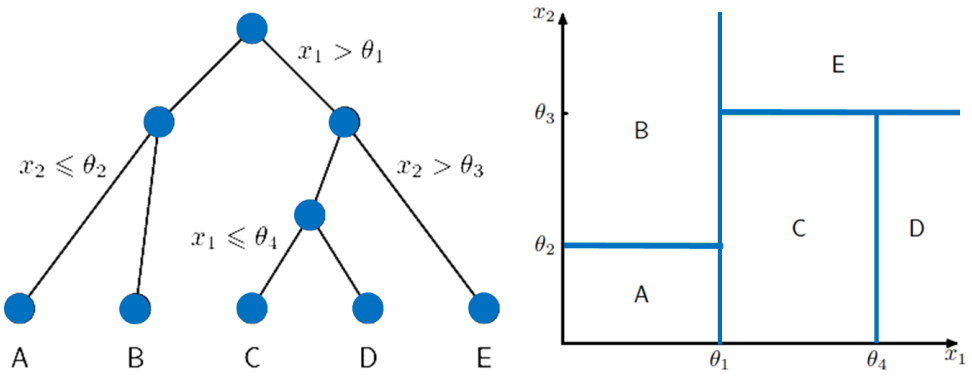

(a) Binary tree. (b) Two-dimensional input space divided.

Figure 3.2: In (a), the binary tree corresponding to the partitioning of input space and in (b) an illustration of a two-dimensional input space that has been partitioned into five regions. Adapted from Bishop et al. [4].

Decision Tree Growth: Let us consider the feature space, whose whole representation can be seen as the top node of the tree. The structure of a Decision Tree corresponds to the nodes and branches contained in it or, in other words, how the feature space is divided. New nodes are added by starting at the root node and applying a split criterion to decide whether the tree branches left or right. This split criterion is decided by taking into account the most representative feature (the one that leads to the minimal expected error of classification) of the input data and comparing it with a splitting variable, by exhaustive search. The splitting criterion can take into account different statistical moments of the input data (as mean, variance or others). After this first branching, we get two child-nodes, each one containing a part of the input data. Further divisions of the feature space occur at each node, with the corresponding input data being branched similarly to what happens in the first node. Both the most representative feature for branching, x_n and splitting variable at each node, θ_n, are depicted in Figure 3.2a. Trees are grown until the expected classification error remains constant or becomes lower than a pre-specified threshold.

Pruning: Bishop et al. [4] state that the none of the available splits produces a significant reduction in error, and yet after several more splits a substantial error reduction is found. For this reason, it is common to grow larger trees, using a stopping criterion based on the number of data

points associated with the leaf nodes, and then prune back the resulting tree. Pruning the tree corresponds to defining the resulting depth of the tree, that is expected to be large enough to allow enough descriptive splittings, but remain as small as possible to avoid redundant branches or over-splitting of the data. More detailed information about the pruning criteria can be found in Bishop et al. [4].

Classification and Clustering: For any new sample to be classified, we determine the subregion in which it falls the most. We start at the top node of the tree and follow a path to the final depth, branching down according to the splitting variables (Bishop et al. [4]). The final predicted label is the most voted terminal region and, for the majority of the applications, this is the only thing that matters. However, the potentialities of decision trees are not restricted to classification, since they naturally cluster the data when splitting. This carries descriptive power about the input data. Such a description can be measured by counting the number of times each subregion is reached by the instances of the data when descending a tree. This inspired the search for tree-based approaches that take advantage of this clustering to generate codebooks of the input data, in machine learning, known as BoW.

Random Forests: Using a single Decision Tree is not a guarantee itself that the different patterns of the data are correctly learned. It has been described that the tree structure is very sensitive to small changes in the dataset, generating variable sets of splits (Friedman et al. [15]). Additionally, the splits on the feature space are parallel to its axes (see Figure 3.2b) which may be suboptimal. It is possible that the most robust split criterion for a specific input data is an oblique threshold, which is not guaranteed by Ordinal Decision Trees, where the splitting criterion is always a constant value on the feature space. We can overcome these drawbacks by using a set of randomly generated Decision Trees, known as RF.

A RF is an ensemble of T decision trees. Associated with each node n in the tree is a learned class distribution $P(c|n)$. The whole forest contributes for the final classification by averaging the class distributions over the terminal nodes nodes $L = (l_1, \ldots, l_T)$ reached for all T trees:

$$P(c|L) = \frac{1}{T} \sum_{t=1}^{T} P(c|l_t) \tag{3.1}$$

RF add randomization to the learning process since each one of the trees is independently generated and assumes a unique set of splitting criteria and branches. This way, the same input data is differently branched and all the relevant splittings are expected to occur. Considering that we cannot guarantee that a single Decision Tree is capable to learn the best classification model without undesired variance and bias (caused by an erroneous parameter tuning), using RF increases the probability of learning the underlying model that discriminates between different classes.

In this work we follow the research of Shotton et al. [48], applying RF to perform the hierarchical clustering of local image patches into a BoW that summarizes the pattern content of the input images. In other words, RF can be perceived as simple spatial partitions that assign a dis-

tinct visual word from the BoW to each leaf (Shotton et al. [48]). This hierarchical clustering is obtained by the successive branches of the input data according to the different splitting criteria: at the first splits we can distinguish heterogeneous patterns of the input data; while approximating the leaf node we increasingly separate more homogeneous patterns, achieving highest levels of descriptiveness.

K-means: K-means is commonly used for clustering the input data by defining random centroids and assigning each instance to a class that corresponds to the closest centroid. The classification is iteratively updated depending on the existing data until the centroids do not change. This is especially useful when we do not have labeled data, making K-means a fair solution for unsupervised learning. Sometimes the best clustering is not possible when the random, and data-independent, initialization of centroids is too different from the real centroids, not converging into an acceptable solution. In this specific application, we are dealing with a dataset previously labeled by specialists. This means that we can explore the hierarchical clustering capabilities of RF to cluster the data with fastness and more stability in the differentiation of different patterns, when compared to K-means (Shotton et al. [48]), since intermediate patterns are considering into the analysis.

3.2 Image Acquisition and Processing

The output of an endoscopy is a video of the structures of the alimentary canal. It is processed by physicians who extract at least one relevant frame, which may have undesired image artifacts. We try to smooth such artifacts by rescaling the images. Then, physicians use custom-made software[1] to define the regions of clinical interest of each image, whose masks were provided and used for segmentation. Here, our methodology can process images with intensities described using four different color space types: RGB, Opponent Space, CIE-LAB and Grayscale. Then, we apply a Gaussian smoothing filter for denoising purposes. These pre-processing steps are represented in the Figure 3.3.

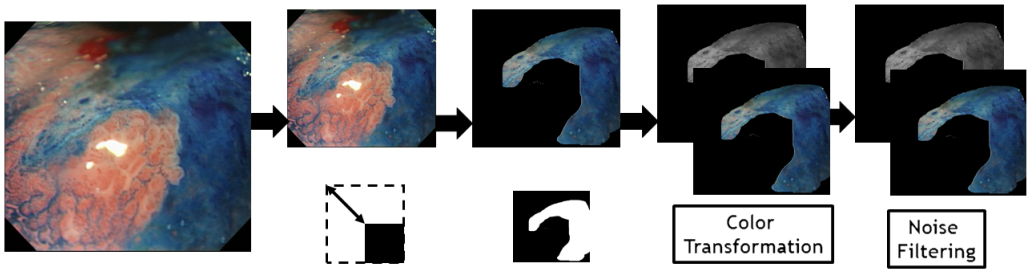

Figure 3.3: Image processing stages of the acquired endoscopy video: frames are merged into a single view, rescaled and segmented though the physician-annotated masks.

[1] Developed at IT - Institute of Telecommunications, Porto.

Following this, we perform a feature extraction stage. As previously mentioned, features are intended to be unique, accurate and distinctive. Our methodology aims at combining such characteristics into a single feature extraction strategy. Nevertheless, in order to achieve this goal some challenges arise.

Gastrointestinal images present tissues with different patterns whether they are healthy or not. Although these patterns are easily identified by a trained physician, the task is much more complicated for other professionals and, especially, computers. This is because common pattern recognition strategies are designed for generic scenes or objects and are not optimized for medical imaging. In this specific application, the quality of the pattern identification can be compromised by acquisition constraints. Therefore, our methodology must be invariant to rotation, luminance and scale and combining spatial information around each pixel with the intensity values to increase the distinctiveness and reliability of the extracted features.

Our approach divides the segmented image into intensity patches of size *n*x*n*, extracted from the annotated region into an array. Since local features have been described to be more robust to spatial variations (Vogel and Schiele [68]) and medical conditions are often recognized by varying patterns, our methodology looks for regional changes on patterns, thus reducing the influence of non-related regions of the image.

Patches can be overlapped or not, depending on the user-defined patch window and spacing between adjacent patches. If the spacing between the patches is lower than the patch size, there are overlapping and consecutive patches share some intensities. Some overlapping may be desired to diminish the spatial variance inside proximal regions. Tissues associated to the same class that are spatially close are expected to have similar texture. By allowing the overlap of patches, we guarantee that similar tissues have more similar patches.

The intensities of each patch are extracted and reshaped into a vector array. This approach is inspired on the strategy presented by Simonyan et al. [51]. However, instead of extracting a circular region, we look for all pixel intensities. This provides additional spatial information to the description of a region pattern.

From here, the feature vector, containing the stored patch information is normalized to guarantee independence from the original intensity range of the image. As a whole, we are anticipating the need to search for, not only, texture information, but also context information. The feature vector is used to initialize RF to generate BoW in the Vocabulary generation stage.

3.3 Visual Representation

RF contain all the possible patterns or visual words —textons— and in the context of our problem, they can be seen as a BoW. If new data is given to the trees in the forest, it splits according to the existence of similar patterns in the visual codebook.

Let us consider a patch that is given to the first tree of the RF. This patch descends the tree, splitting its information left or right, which causes it to cross certain nodes of the tree until it reaches a leaf node. We repeat this in all of the trees and all of the patches extracted from each

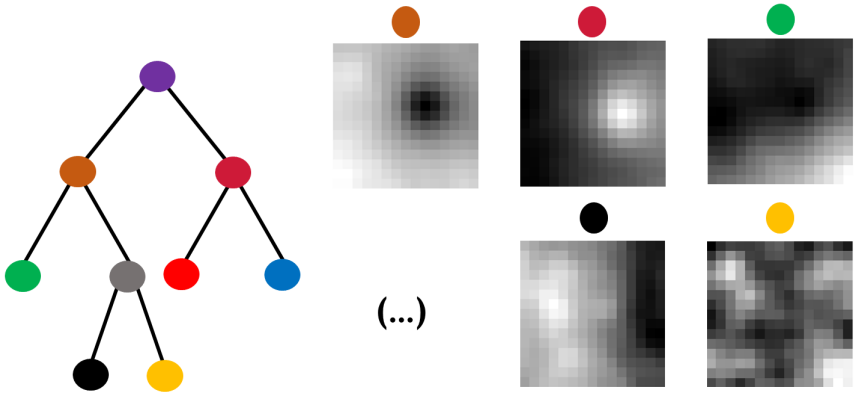

Figure 3.4: Representation of the average-patch that pass in each node. Different patterns are distinguishable in different nodes, suggesting a good separation of the input data into different visual words.

image, counting the number of times each node belongs to a descending path, generating the Vocabulary of the images. Each patch is expected to have different terminal nodes in different trees due to the randomness associated to their generation. However, patches which belong to different images of the same class are expected to cross similar paths along the trees in a forest. This is depicted in Figure 3.4.

The inspection of the RF is provided by the information organized within each tree: (a) an array with the index of the feature vector that corresponds to the most descriptive intensity for each patch at a specific level; (b) a split array, indicating the value for comparison with the intensity identified in (a), allowing to decide the growth direction of the tree; (c) a two-column matrix, the *treemap*, which indicates the next daughter-node in the tree, describing left and right branches.

As a whole, this inspection of the generated RF allows the collection of a set of relevant information which describes the images. We count the number of times each node belongs to the descending path of the patches. This counting vector behaves like a histogram of the visual words and will be the input to build the classifier.

3.4 Image Recognition

We propose the use of SVM for the creation of a classification model, by supervised learning, taking as inputs the training data descriptor and the real class labels. The work that mostly inspired our methodology (Shotton et al. [48]), used RF, not only for hierarchical clustering, but also for classification. However, RF may not be optimized for the classification of medical images: they perform well in static scenes since they take advantage for the distinct features of an objects, not easily confused when we are dealing with common objects (their Vocabulary is highly different). With medical images, this is not true: since all the patterns on the region of interest belong to hu-

man tissue, the differences we are looking at are smooth, not very distinct and we cannot guarantee an accurate distinction using a voting strategy on the terminal nodes (as classification RF do).

SVM were introduced by Vapnik and Vapnik [66] as a tool that fits a binary classification model to the training data, by defining an hyperplane in the feature space that best separates the features of different classes. Additionally, such hyperplane is expected to correctly fit the test data thus dividing it into the two considered classes. From then, SVM have been extensively used in machine learning applications, for image and signal classification.

We are given l training examples $\{x_i, y_i\}$, $i = 1,\ldots, l$, where each example has d inputs $x_i \in \Re^d$, and a class label with one of two values $y_i \in \{-1, 1\}$. Now, all hyperplanes in $\Re^d$ are parametrized by a vector w, and a constant b, expressed as follows:

$$w \cdot x + b = 0 \tag{3.2}$$

Being w the vector orthogonal to the hyperplane. Given such hyperplane (w, b) that separates the data, this gives the function

$$f(x) = sign(w \cdot x + b) \tag{3.3}$$

The hyperplane that best separates the input data into classes can be found by maximizing its distance to the closest data points. The functional distance of each hyperplane is ≥ 1. Each coordinate pair can define each given hyperplane (w, b), but each has a different functional distance to a given data point (Boswell [5]). Therefore, the distance d from the hyperplane candidate to a specific point must be normalized by the magnitude of w, as follows:

$$d((w, b), x_i) = \frac{y_i(x_i \cdot w + b)}{\|w\|} \geq \frac{1}{\|w\|} \tag{3.4}$$

It is intuitive that finding the maximum distance can be achieved by minimizing $\|w\|$. The most commonly used strategy is the usage of Lagrange Multipliers, as described in Vapnik and Vapnik [66]. The more samples we use, the better this stage is. Additionally, the bias parameter, b can be determined taking any positive and negative support vector, x^+ and x^- respectively, as follows:

$$b = -\frac{1}{2}(w \cdot x^+ + w \cdot x^-) \tag{3.5}$$

The proven principle of SVM is that the input data can be perfectly separable. However, in some cases, such separation can only be achieved if the information is mapped into higher dimensions, thus increasing greatly the computational cost. There must be a compromise between the fitting of the best hyperplane and a huge complexity, against a lighter processing stage and the existence of some misclassified samples.

In fact, in real situations, a perfect separation between classes is not always possible. SVM can be tuned using different parameters to achieve the maximum fitting. For this purpose, kernels, power formulas that allow the mapping for higher dimensions, have been designed. Another ex-

ample of tuned parameters is the cost, C, whose value defines the acceptable number of wrongly classified observations during the model fitting. As concluded before: (i) SVM maximize the distance between the hyperplane and the closest points; (ii) we often deal with misclassified observations when defining the margin, especially when the optimal separation between the data is not feasible with low computational cost. Following this, we must define a soft-margin, one that performs and acceptable separation of the data, while allowing some misclassifications to occur. The growth of the margin is critical and controlled by C, the cost of each misclassified sample.

In our specific application, SVM should inspect the Vocabulary and fit the classification model that differentiates the classes of the images. The tuning of SVM parameters will be performed by k-fold cross-validation, to optimize the relation between the regularization parameter and the homogeneous parameter of the kernel. Additionally, an intersection kernel is used to build the model, since the feature vector can be interpreted as a histogram.

Multiclass classification As SVM provide a binary answer to classification problems: an observation either belongs to a specific class or not. In a multi-class problem, such as this one, it is impossible to label all the observations in a single instance. Thus, a multiclass classification strategy must be followed. We have chosen a one-versus-all (OVA) strategy: we compute the probability of a certain observation to belong or not to each of the classes against the others (Sousa et al. [57]) and then the predicted class of an observation is the one with the best score.

Other approaches would be possible, such as the method proposed by Frank and Hall [14]. This approach takes into account a linear relationship between the existing classes, which is not completely true in gastroenterology since the evolution of patterns between different stages of cancer is not linear. Additionally, this solution does not consider that each class is independent from the others, and provides less comparisons than OVA.

Chapter 4

Results and Discussion

In the current Chapter we evaluate the performance of the methodology proposed in Chapter 3, presenting and discussing the results of the experimental study performed. Here, we discuss how the different parameters of each of the stages of our method influences the classification of new instances, or images. In each test, we varied specific parameters, maintaining a standard parameter configuration for the following variables:

- Images were resized to half of their original size and converted to grayscale.
- 100 patches of 5 pixels width, randomly chosen.
- Random Forests with 10 trees, each tree with 100 nodes.
- Intersection kernel and one-versus-all strategy for SVM classification.

All the tests were performed in a AMD Phenom II X4 955 CPu @ 3.20 Ghz, 8GB RAM (64-bit) computer.

4.1 Dataset

Our dataset consists of 176 chromoendoscopic images, pre-segmentated into clinically relevant regions according to manual annotations by an expert physician. This dataset is encompassed by 56 normal tissues and 96 metaplasia and 24 dysplasia cases (see Dinis-Ribeiro et al. [12] for more information). A sample of our dataset is depicted in Figure 4.1. The three images presented there are representative of the aforementioned classes.

It is possible to see different constraints to the analysis of the images in this dataset that must be addressed in this work. The acquired images may be blurred and present specular highlights or fluids. Moreover, there are limitations related with the acquisition procedure: the varying distance between the probe and the tissues, possible rotation of the probe and images with regions without clinical interest.

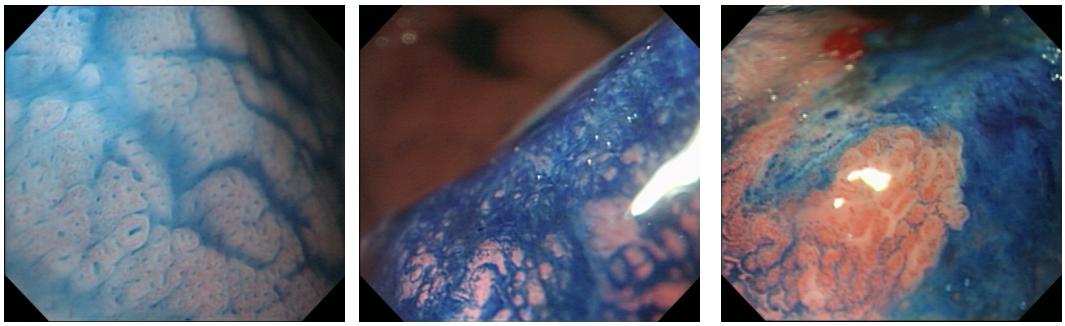

(a) Normal tissue. (b) Tissue with dysplasia. (c) Tissue with metaplasia.

Figure 4.1: Images describing different types of patterns from the gastrointestinal tract that are representative of our dataset

4.2 Methodology and Experimental Study

The dataset presented in previous section will be the object of our study, being randomly divided into train and test images, 30 and 146, respectively, for each test performed. We ensure that each class is similarly represented in the training set in order to allow a similar learning of all the classes. Moreover, we expect similar results for different dataset of gastroenterology images, since the acquisition constraints are similar.

4.2.1 Error and Statistical Significance Assessment

The experiments assessed in the Chapter were evaluated and compared according to the following methodologies.

Performance evaluation: Performance was assessed calculating the error according to:

$$Error = \frac{1}{c} \cdot \sum_{i=1}^{c} \frac{FN_i}{FN_i + TP_i} \tag{4.1}$$

where c is the total number of classes, FN the false negative results and TP the true positives.

Tests were repeated 20 times and the mean error considered.

Statistical Significance: Statistical significance of the results was performed. The different experiments were evaluated statistically in order to find if the difference between the tests is significant or even different or similar.

The normality of the data was ensured by Jarque-Bera tests (Jarque and Bera [26] and Thadewald and Büning [62]) and significance was computed using two-tailed t-tests. We took $p < 0.05$ as criterion for significance.

4.2.2 Image Processing and Feature Extraction

The images were processed and some tests were assessed. Regarding the image processing, we tuned **(a)** the influence of color information and **(b)** the influence of resizing the image before extracting the patches. Tuning the parameters regarding the extraction of information of the images we aim at **(a)** the patch dimensions, **(b)** the influence of extracting and including rotation information in the analysis, **(c)** how to select the more descriptive regions where to extract the patches, **(d)** the amount of valuable information to use for the subsequent stages of processing; and **(e)** which is the best strategy to normalize the data extracted directly from the images.

Color: A color performance study was performed for four color spaces: grayscale, RGB, Opponent Space and CIELab. Our original images are RGB and the conversions are presented below, considering that R, G and B stand, respectively, for the red, green and blue color channels of the image.

As presented in Riaz et al. [45], grayscale images have performed well in gastroenterology field. This can be explained by the existent CV methods which aim at mimic the primary visual cortex, working mainly for detection of shapes by the existent contrast of black and white. We converted RGB images to grayscale according to the following adopted formula (Akenine-Möller et al. [1]):

$$I = 0.3 \times R + 0.59 \times G + 0.11 \times B \tag{4.2}$$

However RGB color space is the most frequent, other spaces were proposed in order to mimic the operation of the human vision system. The opponent color space is an example of this, relying on opponent hues: yellow or blue and red or green. The human vision is not able to detect the opponent colors at the same time and the opponent color space take advantage, transforming RGB in three different channels: Yellow-Blue (YB), Red-Green (RG) and a monochromatic channel (I). Starting from here, effective color features were derived and a basic representation can be obtained by follow(Plataniotis and Venetsanopoulos [42]) :

$$I1 = \frac{R+G+B}{3} \tag{4.3}$$

$$I2 = R - B \tag{4.4}$$

$$I3 = \frac{2G-R-B}{2} \tag{4.5}$$

Methods like the ones presented above perform well in specific applications but not under any circumstances. This create the need for color spaces invariant to operation conditions. In response to that, CIELab, which is also an opponent color space, present 3 color dimensions, L, approximating the human perception o lightness, $a*$ and $b*$ that correspond to RG and YB, respectively.

The transformation from RGB to CIELab was performed using the Mathworks Matlab built-in *rgb2lab* function.

The results of the experiments performed are presented in 4.1.

Table 4.1: Average errors for 20 runs varying the color space.

Image Scale	Average Error	*p*-Value with respect to			
		Grayscale	RGB	OS - standard	OS - CIELab
Grayscale	$23.79(\pm 3.73)\%$	-	0.0001	0.0001	0.0001
RGB	$35.33(\pm 4.71)\%$	-	-	0.0044	0.8309
OS - standard	$39.57(\pm 4.70)\%$	-	-	-	0.0335
OS - CIELab	$35.73(\pm 6.71)\%$	-	-	-	-

Image Filtering : We filtered the images by an isotropic Gaussian kernel, with different sigmas calculated as follows:

$$\sigma = \sqrt{\left(\frac{8}{k}\right)^2 - 0.25} \tag{4.6}$$

where k corresponds to the kernel size.

The value of the sigma varies according to the kernel size; for each kernel we save a patch. This ensures invariance to the illumination.

Image Resizing: We tested the influence of resizing the images of our dataset to 25% and 50% of its original size (518 x 481).

The acquired images have noise and artifacts, which we intend to remove or, at least, reduce during the pre-processing stage. One of the strategies to achieve it is resizing the images. As presented in Table 4.2, when we resize the images to half of its original size, we have a lower error when compared to the full-sized image. However, the means are statistically similar. This suggests that resizing the images to 50% of its size does not compromise the content of the image for classification and reduces the noise, taking into account that the average error decreases. On the other hand, when classifying images resized to a quarter of its original size, we get an error of the same range (slightly higher), however with statistically different means, suggesting that this scale of resizing is harmful: although the image artifacts are smoothed and the computational cost decreases, the relevant information contained in the images also becomes lost, thus compromising the classification.

Feature Extraction: In this stage we aim at extracting relevant information from images, invariant to acquisition constraints. This can be achieved by optimizing the feature extraction parameters to guarantee maximum descriptiveness. The following settings and variables were tested:

- **Patches size:** 5, 11, 15, 21 and 25;

Table 4.2: Average errors for 20 runs varying the scaling of the image between the original size, 50% and 25%.

Image Scale	Average Error	*p*-Value with respect to		
		100%	**50%**	**25%**
100%	$29.92(\pm 3.92)\%$	-	0.3770	0.0001
50%	$23.79(\pm 3.73)\%$	-	-	0.0001
25%	$24.83(\pm 3.43)\%$	-	-	-

- **Image Rotation:** without any rotation (extracting information as obtained in the pre-processing step) and rotating the image and extracting information with 0, 90, 180 and 270 degrees of rotation.

It is relevant to test the patch size to optimize the compromise between the extraction of enough descriptive information and the computational cost. In other words, the extraction of small patches, however fast, may not provide sufficiently discriminative spatial information. The opposite occurs for large patches. A patch, in this context, is a unit of texture and should be capable of representing an existing pattern of the image which is repeated along the images. The optimization of the patch size allows us not to lose or include too much information about the image patterns. Moreover, trying to address the rotation variation that occurs during the acquisition of the images, we rotate them and extract the patches considering different angles. We have evaluated this parameter together with the patch width and the results are presented in Figure 4.2 and Table 4.3. To determine the patch size with the best performance, we computed the average error and statistical significance.

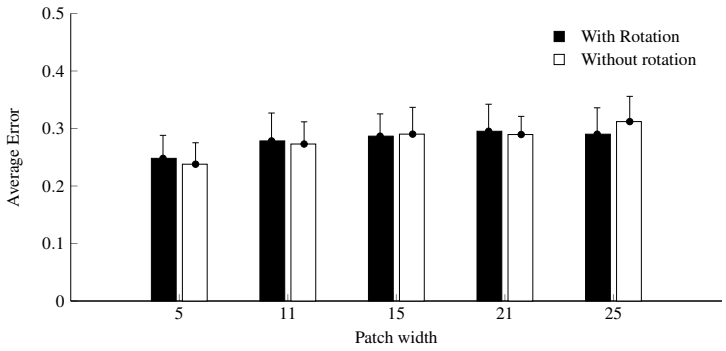

Figure 4.2: Average error with respect to patch width.

The results show that, for patches of the same width, there is no statistical significance between them whether or not rotation information during the patch extraction stage is included, suggesting that the inclusion of rotation is not required for an accurate classification. Additionally, the lowest errors were found for the smallest patch width tested (5-pixels). This evidence together suggests that we are able to extract enough descriptive information while avoiding heavy processing. It is possible that larger patches present multi-pattern information, more difficult to interpret and distinguish by the SVM classifier. This is because the probability of having heterogeneous information

Table 4.3: Average error for 20 runs varying the size of the patch and the extraction of rotation information.

Patch Width	With Rotation	Without Rotation	*p*-Value
5	24.81($\pm$4.00)%	23.79($\pm$3.73)%	0.4207
11	27.84($\pm$4.85)%	27.30($\pm$3.86)%	0.7052
15	28.67($\pm$3.87)%	29.02($\pm$4.66)%	0.8054
21	29.52($\pm$4.70)%	28.95($\pm$3.16)%	0.6657
25	29.01($\pm$4.59)%	31.20($\pm$4.39)%	0.1406

along patches decreases. It would be interesting to study the performance of the methodology for a patch width smaller than 5 pixels.

Patch selection: We also evaluated the preponderance that the number of patches has on the classification task. The literature states that using the most descriptive patches leads to better results than when we use all of the information contained on the images (Simonyan et al. [51]). To test this hypothesis, two different experiments we prepared: **(a)** data randomly chosen; **(b)** usage of a metric that finds the most homogeneous and the most heterogeneous patches using k-means.

The results for the randomly chosen patches are shown in Figure 4.3. Different quantities of patches were extracted. Since the region of interest among images is variable, the number of patches extracted per image varied between 198 and 5538. Analyzing the results, we can perceive that, as expected, the error is higher when too few patches are selected. Furthermore, the average error stabilizes when we reach 200 patches (when not existent, we extract the maximum patches of an image). This means that a larger quantity of data does not, in itself, mean better and more descriptive information. This is highly correlated with the results obtained for the inclusion or non inclusion of rotation information: the fact that we include more information about rotation is not expected to improve the performance of the descriptor if the information is not discriminative enough. In fact, it is not: we are simply looking at the same pattern from different angles. The focus must be on distinguishing between different patterns, rather than assuming that including rotated information can accurately simulate a rotation of the acquisition endoscope. More information will diminish the discriminative capacity of Random Forests, since we have a finite number of nodes. There is no evidence that all the different patterns can be separated, since more data requires more splits (whose number is limited by the number of nodes we have).

The literature predicts that the performance of the classifier is expected to be higher for more descriptive patches, than for all of the extracted information (Simonyan et al. [51]). Following this, and considering that the behavior of the random choice of patches was promising, we tried a methodology for the extraction of both the most homogeneous and the most heterogeneous patches of each image. They are expected to capture, respectively, the global characteristics of the image and small and discriminative variations on patterns between classes.

We started by choosing the patches using the k-means algorithm. Let us consider a cluster of patches: those nearer to the cluster centroid are the most homogeneous; conversely, the farther

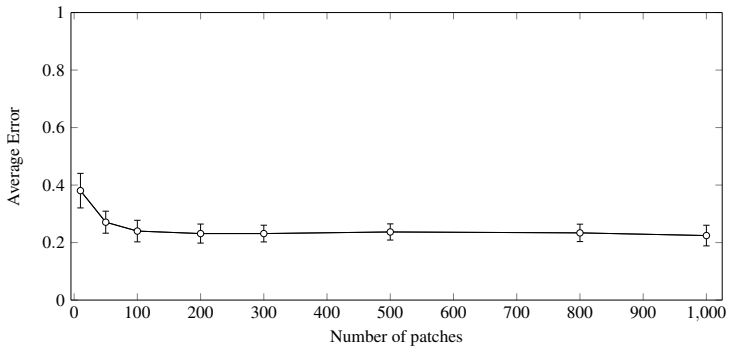

Figure 4.3: Average error with respect to the number of randomly chosen patches.

ones are the most heterogeneous. Although we followed a correct premise, this metric presented some flaws, since the centroids are generated randomly and we cannot guarantee that centroid is representative enough of the homogeneity of the data. We are looking forward to understand how to define the most reliable centroid for clustering and, from there, choose the patches. These flaws cause the metric to perform worse, as expected, and shown in Table 4.4.

Table 4.4: Average Error with respect to patch selection strategy: random selection and approximation to the centroid generating using k-means.

Patch Selection Strategy	**Average Error**
Random Selection	$23.79(\pm 3.73)\%$
k-Means	$47.56(\pm 5.92)\%$
***p*-Value**	0.0001

Patch Normalization: The basic principle of normalization is to map variables that were measured in different scales into the same range, to make a coherent comparison between them possible. Here, we are not dealing with a scale problem. Normalization aims at stabilizing the histogram of the patches, since the pre-processing stages cause them to be saturated in some ranges.

Firstly, we process the patch intensities as follows:

$$p_t(i) = 255 - e^{\frac{m_p - (i)}{m_p} \cdot \log 255} \tag{4.7}$$

where p is a row vector of the pixel intensities previously extracted and m_p is the maximum value inside the patch. After, a new transformation is applied:

$$p_n(i) = \frac{p_t(i)}{\sqrt{\sum_{n=1}^{N} p_t(i)^2 + 2^{-52}}} \tag{4.8}$$

where N is the total number of intensities extracted. After these processing stages, L2 or z-score normalization were tested. The results depicted in Table 4.5 show that normalization is able to improve the performance of our method.

Table 4.5: Average error with respect to the patch normalization.

	p-Value with respect to			Average Error
	No Normalization	*L2*	*z-score*	
No Normalization	-	0.0001	0.0001	$38.45(\pm 5.01)\%$
L2-Normalization	-	-	0.0001	$23.79(\pm 3.73)\%$
z-score Normalization	-	-		$50.04(\pm 3.87)\%$

4.2.3 Random Forest

The BoW was constructed using the Mathworks Matlab R2012b built-in *TreeBagger* function. This function creates an ensemble of decision trees, which we previously named RF (see Section 3.1).

We adapted the function parameters according to the problem at hand:

- We chose Deviance as ***Split Criterion***. While building the trees, the function guarantees the maximum deviance reduction. In other words, it weighs misclassified observations badly optimizing the relevance of each instance.
- ***Pruning*:** was not done. Instead of using the optimal sequence found by pruning the tree using TreeBagger [1], we grew all the trees until the pre-defined number of nodes was reached.

Our approach extends the use of RF presented by Moosmann et al. [37] and Shotton et al. [48]. While these authors only use the information on the leaf nodes, we take advantage from the hierarchical clustering capabilities of the trees, taking into account all the nodes on each tree. The *TreeBagger* function of Matlab outputs unbalanced trees (terminal nodes can be found at any depth and are not grown). Because of this, trees have different configurations and the same node number occurs at different positions. To guarantee that the same node number is attributed to the same position on the tree, we balanced the branches of the trees, introducing new child-nodes in the pruned branches and updating the node number of the already existent ones. This guaranteed that all of the trees had the same structure. The average error obtained using only the terminal nodes of balanced trees to generate BoW was $25.44 \pm 5.03\%$, while an average error of $23.79 \pm 3.73\%$ was obtained using all of the nodes in the trees. This result suggest that the hierarchical clustering is an advantage and using non-terminal nodes provides relevant information that is not captured using only the leaf nodes.

As mentioned before, the randomness of the BoW generation does not always guarantees the best descriptive power of the vocabulary. Different parameters can be varied when looking for an adequate vocabulary while keeping the computational efficiency low:

- **RF dimensions:** 1-10, 50, 100, 200,300 and 500 trees;
- **Number of nodes:** 10, 50, 100, 200, 300, 400, 500, 800 and 1000 nodes.

[1] Mathworks guide for Supervised Learning.

The vocabulary dimensions results from the product of the aforementioned variables. The size of our vocabulary depends both on the number of trees of the forest and the number of nodes on each tree, as explained in Section 3. It influences the computational cost and the accuracy of our methodology, making it necessary to find the best compromise. To address that, we varied both the number of trees and the number of nodes, and the results are shown in Figure 4.4.

The number of nodes determines where the trees stop growing. As previously mentioned, few nodes do not allow the Random Forests to correctly differentiate between the different patterns in the images. Otherwise, for bigger trees, we get redundant data for the final nodes of each tree, providing invaluable data while increasing the computational cost. Regarding the number of trees, as they increase, the strength of the classifier improves since different ways of separating the patterns of the input images are implemented. As always, we must find the ideal number of nodes and the ideal number of trees, so that we can build a robust classifier while reducing the computational cost as much as we can.

Figure 4.4 shows the variation of the average error with the number of nodes of the trees and the size of the RF. It is visible that small trees and forests lead to a poor performance as expected, with increased error and standard deviation. Stabilization of the results occurs for at least 50 trees and 300 nodes. In these conditions, not only does the error but also the standard deviation reach their minimum value.

These results are intuitive because of the reasons mentioned above: too many nodes make the vocabulary redundant and the forest size should allow the robustness of the classifier without compromising the computational cost; additionally, without enough information for the description of images, descriptive power is not ensured. Furthermore, the stabilization values for the number of trees and the number of nodes proves our premisses: we need to increase the number of nodes to a limit for which the information becomes redundant (leading to the stabilization of the average error), and to have the minimum number of trees that guarantees enough randomness to distinguish patterns that the simple splitting of nodes cannot.

Vocabulary Normalization: To normalize the vocabulary we have followed the same strategy adopted to normalize the patch intensities. The results are presented in Table 4.6.

Table 4.6: Average error with respect to the vocabulary normalization.

	p-Value with respect to			**Average Error**
	No Normalization	*L2*	*z-score*	
No Normalization	-	0.0130	0.0978	$23.79(\pm 3.73)\%$
L2-Normalization	-	-	0.5747	$26.89(\pm 3.61)\%$
z-score Normalization	-	-	-	$26.12(\pm 4.70)\%$

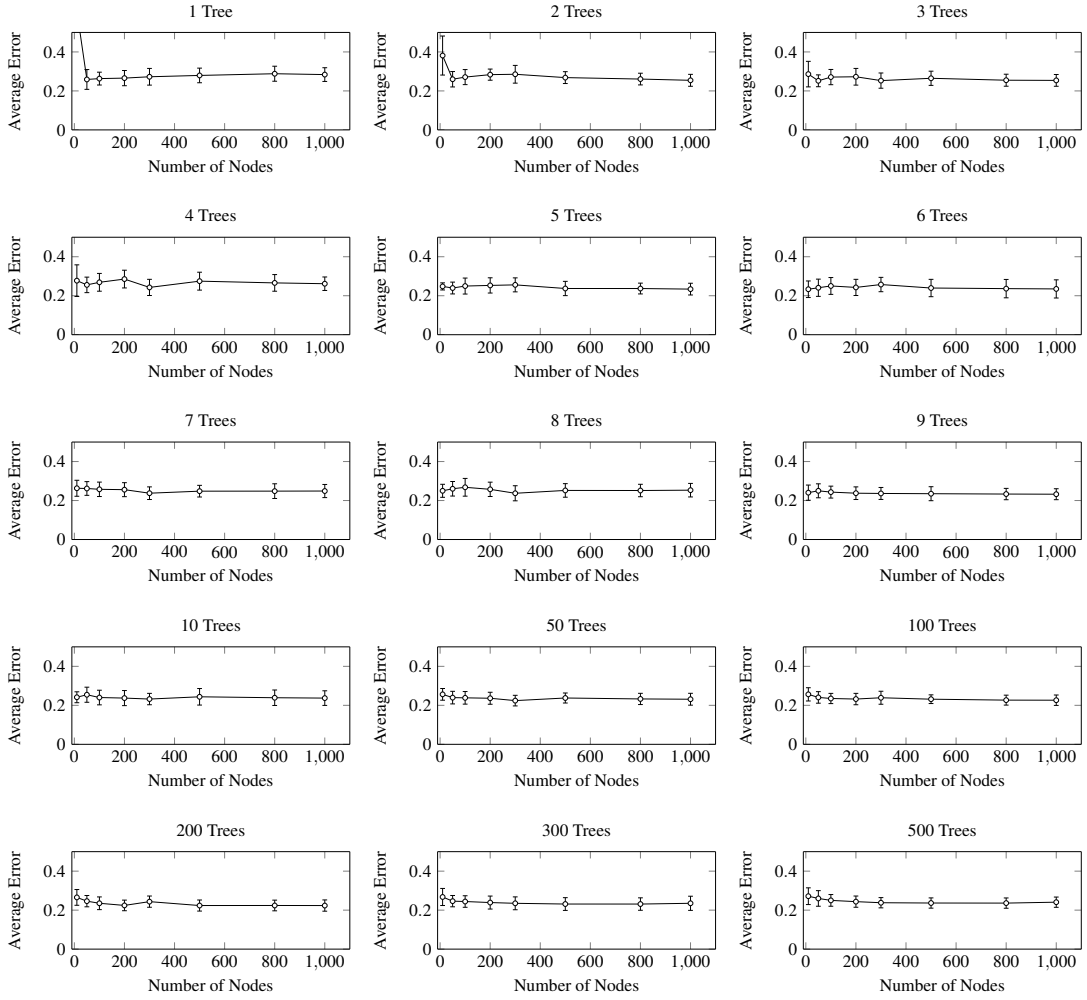

Figure 4.4: Average error variation with respect to the number of nodes and the number of trees.

4.2.4 Recognition of Cancer

We use SVM to construct the classifier, using the VLFEAT[2] built-in *vl_svmtrain* function. Optimal λ and γ parameters were found among the ranges specified below:

- γ: 2^n with n varying between -6 and 0.
- λ: from 0 to 1, with step 0.2

The maximization of the SVM classification power relies on the re-dimension of the feature space as present in this Section. Interesection, χ^2 and Jensen-Shannon kernels (JKS) were tested here[3].

Regarding the classifier construction, the SVM classification model is created using the parameters presented in the Section 3.4. The results in Table 4.7 suggest that using the Histogram

[2] http://www.vlfeat.org

[3] http://www.robots.ox.ac.uk/ vedaldi/assets/pubs/vedaldi11efficient.pdf

Intersection Kernel leads to lower errors, statistically distinguishable from the results obtained applying KJS and χ^2 kernels. This is essentially due to the fact that the vocabulary, obtained after descending the patches along the Random Forest, can be perceived as a histogram: it counts the amount of times each node is crossed by a descending patch. The KJS Kernel takes into account the entropy of the Vocabulary, which is a global statistical metric of the value distribution in a histogram, instead of a direct histogram comparison method. The Intersection and the χ^2 kernels are well-known histogram distance metrics and behave similarly in this specific application. However, lower errors and lower standard deviations are obtained for the Histogram Intersection Kernel, possibly because this metric searches for common regions on the Vocabulary and requiring similar histogram morphologies to have a high intersection value. Conversely, a χ^2 distance value can be low, although corresponding to histograms with very different shapes.

Table 4.7: Average errors and statistical significance values with respect to the generation of a SVM classifier using different kernels.

Classification Kernel	**Average Error**	***p*-Value with respect to**		
		Intersection	χ^2	**JKS**
Intersection	$23.79(\pm 3.73)\%$	-	0.2736	0.0139
χ^2	$25.21(\pm 4.18)\%$	-	-	0.2346
KJS	$26.65(\pm 3.09)\%$	-	-	-

4.3 Best Model Assessment and Discussion

The results presented above allowed us to tune each of the parameters to obtain the lowest possible errors, while keeping the computational cost low. The whole parameter configuration settings for optimal performance is as follows:

- **Resize:** 50% of the original image size;
- **Patch settings:** 5-pixel width, without rotation information;
- **Patch selection:** 200 randomly selected patches, L2-normalized;
- **Random Forest settings:** 50 trees, with 300 nodes each;
- **Vocabulary:** Size 15000, not normalized;
- **SVM classification:** Histogram Intersection Kernel

Table 4.8 presents the confusion matrix obtained when these configurations are applied. An average error of $23.07(\pm 2.83)\%$ was obtained, lower than that obtained by the standard methodologies for gastroenterology image classification. We obtained a small standard-deviation, suggesting high precision of our strategy. Additionally, we can guarantee low errors with low computational cost: the classification of each image takes around 5 seconds to be completed. Translating this to

Table 4.8: Average confusion matrix obtained for this problem, using the optimized parameters of the algorithm. Class "1" refers to the normal tissue images and the "2" and the "3" refer to dysplasia and metaplasia images, respectively. The methodology distinguish better the class "1" from the others than the classes "2" from the "3", suggesting that the major difficulty is in distinguish between classes with clanges.

		Predicted Labels		
		1	**2**	**3**
True Labels	**1**	37	1	1
	2	4	75	4
	3	5	9	10

the medical environment, such performance means that we were able to suggest the classification of a new image acquired in almost real-time, with fast and reliable feedback to physicians. Even if there is the need to acquire new images, the low time required for processing does not interfere with the normal flow of a clinical evaluation.

Performance comparison with Standard Methodology: Here, we show that our methodology has an improved performance, when compared with the standard methodologies used to: extract information and describe gastroenterology images (SIFT); generate a BoW from the image (k-Means). Two major conclusions can be drawn from the results presented in Table 4.9.

When the information is extracted using patches, RF are capable of generating a more robust BoW than k-Means, probably because of the hierarchical clustering of the data. When we extract patches, we gather a lot of information, with highly variable homogeneity. It is not guaranteed that the clustering performed by K-means is capable of distinguishing patches of different classes with similar patterns. we have previously suggested this incapacity in dealing with heterogeneity of the data when patch selection was addressed. By ranking the data using RF, such capacity to distinguish patterns is more probable to occur.

Conversely, k-Means performs better when clustering data extracted using SIFT, in comparison to patch extraction. This is because SIFT extracts prominent features on the image which are indeed expected to be more heterogeneous and variable, easing the clustering for k-Means. The BoW is then more representative and performs slightly better. However, information extracted with SIFT does not lead to the same accuracies when BoW is generated using RF. On one hand, we have less information, and on the other hand it is less representative. In this context, some homogeneity is desirable, since it provides insight about the tissue texture as a whole, better distinguishable when information is extracted through patches.

Two-classes recognition: From the previously presented confusion matrix, we can infer that classes "2" and "3" are more similar between each other, than class 1. It is expected, since they correspond to tissues with some kind of pathology, whereas class "1" stands for normal. Following

Table 4.9: Average error comparing the information extraction stage using SIFT or patch-method, as well as, comparing the BoW method using k-Means and BoW.

		Feature Extraction Strategy		*p-Value*
		Patch	*SIFT*	
BoW Strategy	*RF*	$23.79(\pm 3.70)\%$	$55.79(\pm 7.41)\%$	0.0001
	k-Means	$46.80(\pm 9.82)\%$	$30.44(\pm 4.20)\%$	0.0001
p-Value		0.0001	0.0001	-

this, although dealing with a multiclass approach but we also experimented our methodology for a two-class, using the same dataset: normal tissues versus dysplasia and metaplasia altogether. For this experiment we achieved an average error of 11.03 ± 1.80 %, better than the one presented by Sousa et al. [58], where they use SIFT descriptor combined with K-means. This result suggests that even if the methodology is able to diagnose disease with high accuracy, it is not as aptly to measure the grade of the disease.

Chapter 5

Conclusions and Future Work

Cancer on the gastroenterological tract is a preponderant disease in the current health panorama. As for all kinds of cancer, great effort has been made over the past decades on research and development of technology for diagnosis and treatment. In this context, the diagnosis is not easy because it requires equilibrium between cost, diagnosis accuracy and usability by physicians. Endoscopy is the technique that best meets these requirements and is widely used worldwide for diagnosis. There is a wide variety of endoscope configurations and endoscopic imaging available, but one thing is common to all of them: there is the need for experienced physicians to reduce the subjectivity of the analysis.

Recent developments have introduced computer vision techniques as tools to gain objectivity in such analysis. These methods process the images, looking for distinct features or characteristics capable of acting as fiducial information to distinguish between healthy or cancerous tissues, or event between different stages of the diseases. To achieve this purpose, standard machine learning and image processing methodologies have been explored. Although good performances have been described in the most recent works, these techniques still require human interaction and important input of researchers/operators with respect to what type of features is being searched for. This human intervention is also very important to process the images which present rotation, scale and illumination variations, which are problem that affect the descriptive power of automatic algorithms.

This problems are especially relevant in the analysis of medical images. However, recent computer vision methodologies have addressed these limitations with success in other fields of research. This inspired us to apply one of those methodologies in our approach for gastroenterology image classification. We explored the potentialities of Visual Bagging to automatically learn and describe the images with relevant information that the algorithm identifies and counts during the analysis. We have used Random Forests to generate a Bag of Visual Words for each image, dividing it into patches which descend each tree on the Random Forest, and counted the number of times each node belongs the descending path of the patches. This allowed us to use a robust method to differentiate distinct patterns during the description stage. Instead of a common image descriptor, our approach creates a Vocabulary that is used by SVM for classification.

We performed an experimental study in order to optimize our algorithm configuration and parameters: we aimed at maintaining high accuracy rates while keeping the computational cost low. This is important, since it approximates our tool to its required performance in a medical environment. Using the best set of parameters, we obtained a $23.07 \pm 2.83\%$ average error that suggests: high precision (the standard deviation values are low) and an accuracy that meets the state of the art methods for image classification using descriptors generated using Random Forests. We were able to classify with this error range new input images, taking only 5 seconds per image. This time frame is acceptable and suggest that our methodology can be used for near real-time suggestion on the malignancy of tissues during an endoscopy. We also evaluated the same problem as a two-class challenge, achieving an average error of $11.03 \pm 1.80\%$, competitive to the state of the art methodology for gastroenterology image recognition.

Future work must include the extension of this study including a selection of the most heterogeneous and the most homogeneous patches metric, instead of choosing them randomly. We should study the implementation of a image description stage and new methodologies, capable of extracting relevant color information, since the intermediate stages of cancer present relevant color features (for example, the blue color of tissues is used by physicians as cardinal sign of displasia). Our methodology mimics the mammalian primary visual cortex, responsible to distinguish textures and morphological features (like corners and contours). Color information is addressed by the secondary visual cortex, whose performance cannot be replicable using the currently existing CV techniques. Finally,it would be necessary to study the applicability of our methodology in a medical environment: create a program to be used by physicians as a solution to train their classification skills and to post-process images after an endoscopy to help the diagnosis. Later, we will look forward to extrapolate this method to analyze the video source during an examination. Finally,

Appendix A

Tables of Results

The following pages present tables with all the average error of the experiments presented in Chapter 4.

Table A.1: List of the tests with respective parapeters variation (continuation in Table A.2)

Number of Test	Color	Patch Size	Rotation Information	Resizing Scale	Number of Patches
1	grayscale	5x5	Yes	50%	100
2	grayscale	5x5	No	50%	100
3	grayscale	11x11	Yes	50%	100
4	grayscale	11x11	No	50%	100
5	grayscale	15x15	Yes	50%	100
6	grayscale	15x15	No	50%	100
7	grayscale	21x21	Yes	50%	100
8	grayscale	21x21	No	50%	100
9	grayscale	25x25	Yes	50%	100
10	grayscale	25x25	No	50%	100
11	grayscale	5x5	No	100%	100
12	grayscale	5x5	No	25%	100
13	grayscale	5x5	No	50%	10
14	grayscale	5x5	No	50%	50
15	grayscale	5x5	No	50%	200
16	grayscale	5x5	No	50%	300
17	grayscale	5x5	No	50%	500
18	grayscale	5x5	No	50%	800
19	grayscale	5x5	No	50%	1000
20	grayscale	5x5	No	50%	100
21	grayscale	5x5	No	50%	100
22	grayscale	5x5	No	50%	100
23	grayscale	5x5	No	50%	100
24	grayscale	5x5	No	50%	100
25	grayscale	5x5	No	50%	100
26	grayscale	5x5	No	50%	100
27	grayscale	5x5	No	50%	100
28	RGB	5X5	No	50%	100
29	RGB	5X5	No	50%	200
30	RGB	5X5	No	50%	300
31	RGB	5X5	No	50%	1000
32	RGB	15X15	No	50%	100
33	RGB	15X15	No	50%	200
34	RGB	15X15	No	50%	300
35	RGB	15X15	No	50%	1000
36	Opponent	5X5	No	50%	100
37	CIELab	5X5	No	50%	100
38	grayscale	5x5	No	50%	200

Table A.2: List of the tests with respective parameters variation and average error (continuation in Table A.3).

Number of Test	How choose patches	Patches Normalization	Number of Trees	Number of Nodes
1	randomly	l2-norm	10	100
2	randomly	l2-norm	10	100
3	randomly	l2-norm	10	100
4	randomly	l2-norm	10	100
5	randomly	l2-norm	10	100
6	randomly	l2-norm	10	100
7	randomly	l2-norm	10	100
8	randomly	l2-norm	10	100
9	randomly	l2-norm	10	100
10	randomly	l2-norm	10	100
11	randomly	l2-norm	10	100
12	randomly	l2-norm	10	100
13	randomly	l2-norm	10	100
14	randomly	l2-norm	10	100
15	randomly	l2-norm	10	100
16	randomly	l2-norm	10	100
17	randomly	l2-norm	10	100
18	randomly	l2-norm	10	100
19	randomly	l2-norm	10	100
20	k-means	l2-norm	10	100
21	randomly	z-score	10	100
22	randomly	no	10	100
23	randomly	l2-norm	10	100
24	randomly	l2-norm	10	100
25	randomly	l2-norm	10	100
26	randomly	l2-norm	10	100
27	randomly	l2-norm	10	100
28	randomly	l2-norm	10	100
29	randomly	l2-norm	10	100
30	randomly	l2-norm	10	100
31	randomly	l2-norm	10	100
32	randomly	l2-norm	10	100
33	randomly	l2-norm	10	100
34	randomly	l2-norm	10	100
35	randomly	l2-norm	10	100
36	randomly	l2-norm	10	100
37	randomly	l2-norm	10	100
38	randomly	l2-norm	50	300

Table A.3: List of the tests with respective parameters variation and average error.

Number of Test	Vocab. Norm.	Kernel Classif	Classif strategy	Average Error	Standard Deviation
1	No	interesec	OVA	24,81%	4,00%
2	No	interesec	OVA	23,79%	3,73%
3	No	interesec	OVA	27,84%	4,85%
4	No	interesec	OVA	27,30%	3,86%
5	No	interesec	OVA	28,67%	3,87%
6	No	interesec	OVA	29,02%	4,66%
7	No	interesec	OVA	29,52%	4,70%
8	No	interesec	OVA	28,95%	3,16%
9	No	interesec	OVA	29,01%	4,59%
10	No	interesec	OVA	31,20%	4,39%
11	No	interesec	OVA	29,92%	3,92%
12	No	interesec	OVA	24,83%	3,43%
13	No	interesec	OVA	38,06%	6,01%
14	No	interesec	OVA	27,90%	3,83%
15	No	interesec	OVA	23,13%	3,31%
16	No	interesec	OVA	23,13%	2,91%
17	No	interesec	OVA	23,69%	2,81%
18	No	interesec	OVA	23,37%	3,03%
19	No	interesec	OVA	22,44%	3,59%
20	No	interesec	OVA	47,56%	5,92%
21	No	interesec	OVA	50,04%	3,87%
22	No	interesec	OVA	38,45%	5,01%
23	l2-norm	interesec	OVA	26,89%	3,61%
24	z-score	interesec	OVA	26,12%	4,70%
25	No	JKS	OVA	26,65%	3,09%
26	No	Chi-2	OVA	25,21%	4,18%
27	No	interesec	Frank&Hall	35,13%	4,05%
28	No	interesec	OVA	35,33%	4,71%
29	No	interesec	OVA	34,17%	4,71%
30	No	interesec	OVA	33,94%	5,50%
31	No	interesec	OVA	35,98%	4,71%
32	No	interesec	OVA	36,98%	4,71%
33	No	interesec	OVA	61,07%	5,50%
34	No	interesec	OVA	38,15%	6,67%
35	No	interesec	OVA	34,54%	6,39%
36	No	interesec	OVA	39,57%	4,70%
37	No	interesec	OVA	35,73%	6,71%
38	No	interesec	OVA	23,07%	5,01%

Table A.4: List of the tests with respective parameters variation and average error (continuation in Table A.5).

Test Name	Color	Patch Size	Rotation Information	Resizing Scale Scale	Number of Patches
Patch + K-means	grayscale	5x5	No	50%	100
SIFT+RF	grayscale	5x5	No	50%	100
SIFT+Kmeans	grayscale	5x5	No	50%	100
Leaf nodes	grayscale	5x5	No	50%	-

Table A.5: List of the tests with respective parameters variation and average error (continuation in Table A.6).

Test Name	How choose Parches	Patches Normalization	Number of Trees	Number of Nodes
Patch + K-means	randomly	l2-norm	10	100
SIFT+RF	randomly	l2-norm	10	100
SIFT+Kmeans	randomly	l2-norm	10	100
Leaf nodes	randomly	l2-norm	10	100

Table A.6: List of the tests with respective parameters variation and average error.

Test Name	Vocabulary Normalization	Kernel Classif	Classif Strategy	Average Error	Standard Deviation
Patch + K-means	No	interesec	OVA	46,80%	9,82%
SIFT+RF	No	interesec	OVA	55,79%	7,40%
SIFT+Kmeans	No	interesec	OVA	30,44%	4,20%
Leaf nodes	No	interesec	OVA	25,44%	5,03%

Table A.7: Average error varying the number of trees of the RF and number of nodes for tree (continuation in Table A.8).

		Number of Nodes							
		10		**50**		**100**		**200**	
		Average	**SD**	**Average**	**SD**	**Average**	**SD**	**Average**	**SD**
Number of Trees	**1**	61.07%	5.35%	25.88%	5.08%	26.32%	3.29%	26.57%	3.90%
	2	38.15%	10.01%	25.99%	3.95%	27.09%	3.86%	28.35%	2.86%
	3	28.62%	6.55%	25.19%	3.04%	27.10%	3.91%	27.26%	4.28%
	4	27.73%	8.11%	25.56%	3.98%	26.88%	4.56%	28.54%	4.55%
	5	24.78%	1.82%	23.95%	3.03%	24.96%	4.10%	25.29%	3.91%
	6	23.32%	4.25%	24.09%	4.42%	25.01%	4.32%	24.26%	4.15%
	7	26.29%	4.10%	26.18%	3.52%	25.75%	3.70%	25.57%	3.59%
	8	24.99%	3.34%	26.03%	3.73%	26.79%	4.55%	25.74%	3.68%
	9	24.04%	3.90%	24.99%	3.58%	24.32%	3.06%	23.76%	3.24%
	10	24.14%	2.80%	25.44%	3.87%	24.00%	3.75%	23.72%	3.87%
	50	25.63%	3.00%	23.96%	3.23%	23.85%	3.23%	23.63%	3.07%
	100	25.63%	3.40%	24.06%	2.96%	23.51%	2.62%	23.22%	2.92%
	200	26.53%	4.04%	24.61%	2.90%	23.52%	3.26%	24.36%	2.88%
	300	26.75%	4.38%	24.61%	2,90%	24.42%	2.96%	23.89%	3.33%
	500	27.15%	4.29%	24.61%	2,90%	24.42%	2.96%	24.36%	2.88%

Table A.8: Average error varying the number of trees of the RF and number of nodes for tree.

		Number of Nodes							
		300		**500**		**800**		1000	
		Average	**SD**	**Average**	**SD**	**Average**	**SD**	**Average**	**SD**
Number of Nodes	**1**	27.26%	4.28%	27.94%	3.75%	28.82%	3.85%	28.38%	3.52%
	2	28.54%	4.55%	26.83%	3.04%	26.08%	3.00%	25.44%	3.06%
	3	25.29%	3.91%	26.48%	3.64%	25.49%	3.08%	25.40%	3.02%
	4	24.26%	4.15%	27.47%	4.59%	26.58%	4.27%	26.16%	3.46%
	5	25.57%	3.59%	23.71%	3.66%	23.69%	2.77%	23.39%	3.01%
	6	25.74%	3.68%	23.95%	4.45%	23.64%	4.71%	23.49%	4.66%
	7	23.76%	3.24%	24.80%	2.99%	24.82%	3.77%	24.87%	3.37%
	8	23.72%	3.87%	25.18%	3.48%	25.14%	3.19%	25.31%	3.47%
	9	23.63%	3.07%	23.50%	3.59%	23.32%	2.91%	23.24%	2.81%
	10	23.22%	2.92%	24.38%	4.24%	23.90%	3.97%	23.71%	3.75%
	50	22.42%	2.72%	23.76%	2.57%	23.28%	2.88%	23.13%	3.04%
	100	23.89%	3.33%	23.15%	2.23%	22.67%	2.55%	22.63%	2.67%
	200	24.36%	2.88%	22.36%	2.84%	22.39%	2.74%	22.35%	2.89%
	300	24.36%	2.88%	23.13%	3.27%	23.12%	3.19%	23.51%	3.63%
	500	24.36%	2.88%	23.65%	2.63%	23.61%	2.64%	24.08%	2.63%

Appendix B

IJUP Abstract

The following page presents the abstract document submitted for the IJUP - Investigação Jovem da Universidade do Porto. Additionally, a part of the work developed in the aim of this project was exposed in IJUP 2015 in an oral presentation.

Recognition of Cancer using a Bag-of-Words Random Forest for Gastroenterology

S. Francisco[1,2], Miguel T. Coimbra [2,5], R. Gamelas Sousa [3,4]

[1] Faculdade de Engenharia, Universidade do Porto, Portugal.
[2] Instituto de Telecomunicações, Porto, Portugal.
[3] Instituto de Investigação e Inovação em Saúde, Universidade do Porto, Portugal
[4] Instituto de Engenharia Biomédica (INEB), Porto, Portugal
[5] Faculdade de Ciências, Universidade do Porto, Portugal

In gastroenterology, Computer Aided Diagnosis techniques have allowed physicians to analyze endoscopic images as a first or second opinion, or even as an educational program [4]. Cancer recognition in the gastroenterology track is such a difficult problem that only trained physicians can easily detect. Some pattern recognition solutions have already been published in the past [1-4]. However, these solutions have to be invariant to acquisition constraints (rotation, scale and luminance), goals which are not always achieved.

We extract features from pre-processed endoscopic images, extracted pixel intensities of some regions, and then use Random Forests to create a Bag of Feature Words (BoW). The BoW is built by counting how many times each feature appears on each image, thus giving its information content, and used to build a classification model using Support Vector Machines.

Our dataset 176 chromoendoscopy images of the oesophagus (30 for training and the remainder for testing), exhibiting three different conditions (normal and the pathological tissues with dysplasia and metaplasia). After 50 runs, we achieve 22.03±3.09% of average error. This results are promissory, especially when compared to the usage of SIFT descriptor and k-means (32.20±3.58%) to generate the BoW for classification.

Our methodology seems to deal well with few data train samples and it is statistically different and better then the results of the existent methodologies.

References:

[1] Sousa, R et al.., Moura, D.C., Ribeiro, M.D. and Coimbra, M.T. (2014), *Local self similar descriptors: Comparison and application to gastroenterology images*, Engineering in Medicine and Biology Society (EMBC), pp. 4635-4638.

[2] Riaz, F. et al., Silva, F.B., Ribeiro, M.D., and Coimbra, M.T. (2012), *Invariant gabor texture descriptors for classification of gastroenterology images*, Biomedical Engineering, IEEE Transactions, v. 59, n. 10, pp. 2893-2904.

[3] Gross, S., Trautwein, C., Behrens, A., Winograd, R., Palm, S., Lutz, H.H., Sokhan, R.S., Hecker, H., Aach, T. and Tischendorf J.J.W.et al. (2011), *Computer-based classification of small colorectal polyps by using narrow-band imaging with optical magnification*, Gastrointestinal endoscopy 74.6, pp. 1354-1359.

[4] Balbaque, F.S., Ribeiro, M.D., Rabenstein, T., Goda, K., Kiesslich, R., Harigsma, J., Edebo, A., Toth, E., Soares, J., Areia, M., Lundell, L. and Marschall, H.U. et al.(2013), *Endoscopic assessment and grading of Barrett's esophagus using magnification endoscopy and narrow band imaging: Impact of structured learning and experience on the accuracy of the Amsterdam classification system*, Scandinavian journal of gastroenterology, v. 48, n. 2, pp. 160-167.

Appendix C

Summary Paper

The following pages present the two-pages summary paper of this Dissertation. It is also available in http://sarafranciscothesis.pt.vu/.

Recognition of Cancer using Random Forests as a Bag-of-Words Approach for Gastroenterology

Sara Francisco* Ricardo G. Sousa (orientador)† Miguel T. Coimbra (co-orientador)‡

***Resumo*—Recognition of cancer in gastroenterology (GE) images is a challenging task, in which only trained physicians succeed. Computer Aided Diagnosis systems have been applying pattern recognition strategies in this context to act as a first or second opinion to help physicians. However, such solutions are self-tailored and affected by image acquisition constraints. We propose a methodology that automatically renders representative features for gastroenterology images from a Bag of Words (BoW) generated with Random Forests (RF). Our experimental study is made over a multiclass dataset of chromoendoscopy images. An optimal average error of $23.07 \pm 2.83\%$ was obtained, while keeping the computational time low, suggesting usability in a medical context and outperforming the standard approaches in this application.**

***Index Terms*—Bag-of-Words, Computer Vision, Endoscopy, Random Forests**

I. Introduction

EVERY year, 2.8 million people are diagnosed with cancer in the gastrointestinal tract and around 1.8 million die of it. Recent studies have shown that the survival rates are especially high for early diagnosis of this cancer, motivating the search for novel, objective and quantitative methods to help medical teams on this task. Computer Vision (CV) solutions have been applied to the classification of endoscopic images with usefulness, adding a quantitative evaluation to the well-established, accurate and minimally invasive endoscopic procedure. However, the endoscopic image acquisition is affected by several constraints which difficult the recognition of cancer recognition and reduce the applicability of some of those CV methodologies.

Currently, the classification of GE images is done by extracting distinctive features from the images, either on the frequency domain (i.e., Gabor filters) or in the spatial domain (i.e., SIFT descriptor), and feeding it to classification models using Support Vector Machines (SVM) or k-NN. Although presenting promising results, such methods can still be improved in terms of descriptiveness and accuracy. Additionally, it would be important to dismiss the need for an user to tune the algorithm parameters, making its definition automatic and adaptable to new datasets. For that, in this work we extend recent advances in CV to the analysis of GE images. Such approaches are commonly used to recognize objects in cluttered scenes by creating a (sparse) histogram of occurrences (vocabulary) of each different pattern (visual word) in the images. A set of visual words is known as BoW and describes the content and frequency of each pattern on an image. This introduces new information to the analysis: not only we know which patterns occur, but also how many times and how different they are.

Different approaches can be used to generate a BoW of the input data. Here, we propose the usage of RF to perform an hierarchical clustering of input pixel-intensities towards the creation of a BoW, in which each visual word corresponds to a unique and distinct pattern on the endoscopic image. A RF is an ensemble of Decision Trees (DT). DT are statistical approaches designed for decision support strategies. They take the input data and subject it to a sequence of binary decisions. This sequence is an iterative approach of sub-decisions that partition the feature space. With a single DT the different patterns of the data are not correctly learned [1]. However, using RF, we add randomization to the learning process and improve the probability to have a more reliable model. RF have been applied to generate BoW by [2], however their usage in GE has not been studied yet. A similar approach has already been tested in GE by [3], but using SIFT and k-means to generate the BoW.

II. Methodology

In this section, we describe the proposed processing pipeline (presented in Figure 1) for the analysis and classification of GE images. The pivotal stage of our method consist in the construction of a vocabulary of the input data, using a BoW created from input pixel intensities using RF.

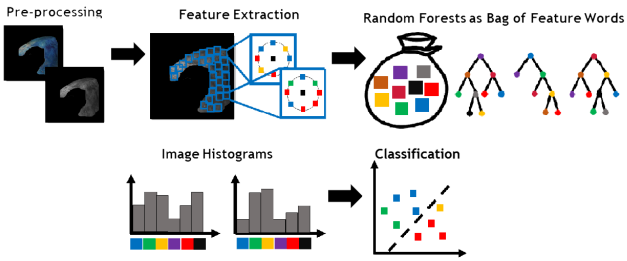

Figura 1: Overview of the pipeline of our methodology to build a classifier model for gastroenterology images.

A. Image Acquisition and Processing

Endoscopic images are acquired during an examination of the inner cavities of the gastric channel, and regions of interest (ROI) are delimited by physicians. For denoising purposes, images are resized and smoothed using a Gaussian low-pass

* saraimfrancisco@gmail.com
† Post-Doctoral Researcher, I3S, INEB, rjgsousa@gmail.com
‡ Auxiliary Professor, FCUP, IT, mtcoimbra@gmail.com

filter. Then, we subdivide the ROI into patches of different sizes containing the pixel intensities of the image.

B. Visual Representation

We generate a BoW using RF. Here, each patch descends each of the decision trees on the forest, until a leaf node is reached. We repeat this process to all of the trees and patches and count the number of times each node belongs to a descending path, resulting in the vocabulary, our representation of the images from which we construct the classifier. The vocabulary can be perceived as an histogram of the visual words and quantize the occurrence of each pattern in the image.

C. Image Recognition

We use SVM to classify the images. The classification model is generated by supervised learning and cost parameters are defined by 3-folds Cross-Validation. Since we are are dealing with a multiclass problem, with different cancer stages (normal tissues, tissues with metaplasia and tissues with displasia), we applied a One-versus-All (OVA) strategy.

III. Results and Discussion

A. Dataset

Our dataset consisted of 176 chromoendoscopic images, pre-segmentated into clinically relevant regions, according to manual annotations by an expert physician. This dataset is encompassed by 56 normal tissues and 96 metaplasia and 24 dysplasia cases (see [4] for more information).

B. Image Processing and Information Extraction

Conversion to grayscale lead to lower errors when compared to RGB, Opponent Space and CIE-lab conversions. Existing CV techniques for image classification cannot assess relevant color information [5], which may explain the results. The influence of patch width and number were tested. The best performances were obtained for small patch widths, 5×5, and 200 patches, randomly chosen. These results suggest that we were able capture the pattern diversity on the images with low computational cost. Small portions of the input data, randomly chosen and without incorporating rotation information, provide a reliable general description of the image. We studied the influence of patch normalization and concluded that L2-normalization lead to better results.

C. Random Forests

The vocabulary dimension and the performance of our methodology is highly influenced by the number of nodes per tree and the number of trees of the RF. The best performance was found for 50 trees, with 300 nodes each, guaranteeing enough randomness on the forest to capture the pattern diversity on the images, and an intermediate number of nodes to avoid redundant branches when a patch descends a tree. Such evidence is shown in Figure 2. Better results were obtained when the vocabulary was not normalized.

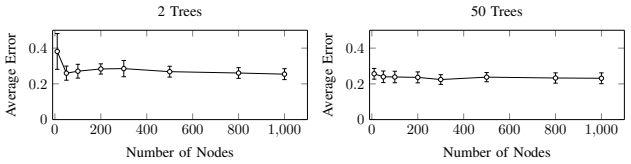

Figura 2: Average error variation for different number of nodes and trees.

D. Recognition of cancer

The intersection kernel of the input data was also found to perform slightly better than χ^2 and JKS kernels [6]. The input data is seen as histograms, making an operation of similarity of histograms potentially better

E. Whole Methodology

We compared the methodology here proposed using the best parametrization with the methodology presented by [3], which uses standard feature extraction and BoW generation methods (respectively, patch extraction and RF *versus* SIFT and k-means). We obtained a $23.79 \pm 3.70\%$ average error, versus a $30.44 \pm 4.20\%$ average error using the standard methodology. The results suggest that our methodology is competitive, especially taking into consideration that each new input image needs around 5 seconds to be classified, allowing near real-time feedback to physicians with reliability. Furthermore, we eliminated the distinction between metaplasia and displasia, and assessed the cancer recognition using only normal and pathological tissues. An average error of $11.03 \pm 1.80\%$ was obtained.

IV. Conclusions

We developed a new methodology that explores the hierarchical clustering capacity of RF to generate a BoW and classify GE images. We improved upon the standard methodologies for cancer recognition in this context, with a low average error of classification and low processing time for each new image.

References

[1] J. Friedman, T. Hastie, and R. Tibshirani, *The elements of statistical learning*. Springer series in statistics Springer, Berlin, 2001, vol. 1.

[2] J. Shotton, M. Johnson, and R. Cipolla, "Semantic texton forests for image categorization and segmentation," in *Computer vision and pattern recognition, 2008. CVPR 2008. IEEE Conference on*. IEEE, 2008, pp. 1–8.

[3] R. Sousa, D. C. Moura, M. Dinis-Ribeiro, and M. T. Coimbra, "Local self similar descriptors: Comparison and application to gastroenterology images," in *Engineering in Medicine and Biology Society (EMBC), 2014 36th Annual International Conference of the IEEE*. IEEE, 2014, pp. 4635–4638.

[4] M. Dinis-Ribeiro, A. da Costa-Pereira, C. Lopes, L. Lara-Santos, M. Guilherme, L. Moreira-Dias, H. Lomba-Viana, A. Ribeiro, C. Santos, J. Soares *et al.*, "Magnification chromoendoscopy for the diagnosis of gastric intestinal metaplasia and dysplasia," *Gastrointestinal endoscopy*, vol. 57, no. 4, pp. 498–504, 2003.

[5] F. Riaz, F. B. Silva, M. D. Ribeiro, and M. T. Coimbra, "Impact of visual features on the segmentation of gastroenterology images using normalized cuts," *Biomedical Engineering, IEEE Transactions on*, vol. 60, no. 5, pp. 1191–1201, 2013.

[6] A. Vedaldi and A. Zisserman, "Efficient additive kernels via explicit feature maps," *Pattern Analysis and Machine Intelligence, IEEE Transactions on*, vol. 34, no. 3, pp. 480–492, 2012.

Bibliography

[1] Tomas Akenine-Möller, Eric Haines, and Naty Hoffman. *Real-time rendering*. CRC Press, 2008.

[2] Miguel Areia, Rita Carvalho, Ana Teresa Cadime, Francisco Rocha Gonçalves, and Mário Dinis-Ribeiro. Screening for gastric cancer and surveillance of premalignant lesions: a systematic review of cost-effectiveness studies. *Helicobacter*, 18(5):325–337, 2013.

[3] G Berci and KA Forde. History of endoscopy. *Surgical endoscopy*, 14(1):5–15, 2000.

[4] Christopher M Bishop et al. *Pattern recognition and machine learning*, volume 4. springer New York, 2006.

[5] D Boswell. Introduction to support vector machines: University of carlifornia. *San Diego*, 2002.

[6] Ken Chatfield, Victor Lempitsky, Andrea Vedaldi, and Andrew Zisserman. The devil is in the details: an evaluation of recent feature encoding methods. 2011.

[7] R Coriat, A Chryssostalis, JD Zeitoun, J Deyra, M Gaudric, F Prat, and S Chaussade. Computed virtual chromoendoscopy system (fice): a new tool for upper endoscopy? *Gastroentérologie clinique et biologique*, 32(4): 363–369, 2008.

[8] James L Crowley and Alice C Parker. A representation for shape based on peaks and ridges in the difference of low-pass transform. *Pattern Analysis and Machine Intelligence, IEEE Transactions on*, (2):156–170, 1984.

[9] Gabriella Csurka, Christopher Dance, Lixin Fan, Jutta Willamowski, and Cédric Bray. Visual categorization with bags of keypoints. In *Workshop on statistical learning in computer vision, ECCV*, volume 1, pages 1–2. Prague, 2004.

[10] Wouter L Curvers, Lorenza Alvarez Herrero, Michael B Wallace, Louis-Michel Wong Kee Song, Krish Ragunath, Herbert C Wolfsen, Ganapathy A Prasad, Kenneth K Wang, Venkataraman Subramanian, Bas LAM Weusten, et al. Endoscopic tri-modal imaging is more effective than standard endoscopy in identifying early-stage neoplasia in barrett's esophagus. *Gastroenterology*, 139(4):1106–1114, 2010.

[11] M Dhanalakshmi, N Sriraam, G Ramya, N Bhargavi, and V Tamizhtennagaarasi. Computer aided diagnosis for enteric lesions in endoscopic images using anfis. *International Journal of Wisdom Based Computing*, 2(1), 2012.

[12] Mário Dinis-Ribeiro, Altamiro da Costa-Pereira, Carlos Lopes, Lúcio Lara-Santos, Mateus Guilherme, Luís Moreira-Dias, Helena Lomba-Viana, Armando Ribeiro, Costa Santos, José Soares, et al. Magnification chromoendoscopy for the diagnosis of gastric intestinal metaplasia and dysplasia. *Gastrointestinal endoscopy*, 57(4): 498–504, 2003.

[13] Jacques Ferlay, Isabelle Soerjomataram, Rajesh Dikshit, Sultan Eser, Colin Mathers, Marise Rebelo, Donald Maxwell Parkin, David Forman, and Freddie Bray. Cancer incidence and mortality worldwide: sources, methods and major patterns in globocan 2012. *International Journal of Cancer*, 2014.

[14] Eibe Frank and Mark Hall. *A simple approach to ordinal classification*. Springer, 2001.

[15] Jerome Friedman, Trevor Hastie, and Robert Tibshirani. *The elements of statistical learning*, volume 1. Springer series in statistics Springer, Berlin, 2001.

[16] Mikihiro Fujiya, Kentaro Moriichi, Nobuhiro Ueno, Yusuke Saitoh, and Yutaka Kohgo. Autofluorescence imaging for diagnosing intestinal disorders. *Colonocopy/Book*, 1, 2011.

[17] Dennis Gabor. Theory of communication. part 1: The analysis of information. *Journal of the Institution of Electrical Engineers-Part III: Radio and Communication Engineering*, 93(26):429–441, 1946.

[18] Sebastian Gross, Thomas Stehle, Alexander Behrens, Roland Auer, Til Aach, Ron Winograd, Christian Trautwein, and Jens Tischendorf. A comparison of blood vessel features and local binary patterns for colorectal polyp classification. In *SPIE Medical Imaging*, pages 72602Q–72602Q. International Society for Optics and Photonics, 2009.

[19] Michael Haefner, Leonhard Brunauer, Hannes Payer, Robert Resch, Alfred Gangl, Andreas Uhl, Friedrich Wrba, and Andreas Vécsei. Computer-aided classification of zoom-endoscopical images using fourier filters. *Information Technology in Biomedicine, IEEE Transactions on*, 14(4):958–970, 2010.

[20] Michael Häfner, Alfred Gangl, Michael Liedlgruber, Andreas Uhl, Andreas Vécsei, and Friedrich Wrba. Classification of endoscopic images using delaunay triangulation-based edge features. In *Image Analysis and Recognition*, pages 131–140. Springer, 2010.

[21] Rehan Haidry and Laurence Lovat. *Medical Imaging in Clinical Practice: Novel Imaging Techniques in Gastrointestinal Endoscopy in the Upper Gastrointestinal Tract*. InTech Open, 2013.

[22] Robert M Haralick, Karthikeyan Shanmugam, and Its' Hak Dinstein. Textural features for image classification. *Systems, Man and Cybernetics, IEEE Transactions on*, (6):610–621, 1973.

[23] Chris Harris and Mike Stephens. A combined corner and edge detector. In *Alvey vision conference*, volume 15, page 50. Manchester, UK, 1988.

[24] Sebastian Hegenbart, Andreas Uhl, Andreas Vécsei, and Georg Wimmer. Scale invariant texture descriptors for classifying celiac disease. *Medical image analysis*, 17(4):458–474, 2013.

[25] Janusz AZ Jankowski and Ernest T Hawk. *Handbook of Gastrointestinal Cancer*. Wiley Online Library, 2013.

[26] Carlos M Jarque and Anil K Bera. Efficient tests for normality, homoscedasticity and serial independence of regression residuals. *Economics letters*, 6(3):255–259, 1980.

[27] Yulei Jiang, Robert M Nishikawa, Robert A Schmidt, Charles E Metz, Maryellen L Giger, and Kunio Doi. Improving breast cancer diagnosis with computer-aided diagnosis. *Academic radiology*, 6(1):22–33, 1999.

[28] Cyrus R Kapadia. Gastric atrophy, metaplasia, and dysplasia: a clinical perspective. *Journal of clinical gastroenterology*, 36(5):S29–S36, 2003.

[29] Hiroyuki Kodama, Fumihiko Yano, Satoki P Ninomija, Y Sakai, and S Ninomiya. A digital imaging processing method for gastric endoscope picture. In *System Sciences, 1988. Vol. IV. Applications Track., Proceedings of the Twenty-First Annual Hawaii International Conference on*, volume 4, pages 277–282. IEEE, 1988.

[30] Shinya Kodashima and Mitsuhiro Fujishiro. Novel image-enhanced endoscopy with i-scan technology. *World journal of gastroenterology: WJG*, 16(9):1043, 2010.

[31] Wen-Jia Kuo, Ruey-Feng Chang, Woo Kyung Moon, Cheng Chun Lee, and Dar-Ren Chen. Computer-aided diagnosis of breast tumors with different us systems. *Academic radiology*, 9(7):793–799, 2002.

[32] Hoo-Yeon Lee, Eun-Cheol Park, Jae Kwan Jun, Kui Son Choi, and Myung-Il Hahm. Comparing upper gastrointestinal x-ray and endoscopy for gastric cancer diagnosis in korea. *World Journal of Gastroenterology*, 16(2):245, 2010.

[33] Baopu Li and MQ-H Meng. Tumor recognition in wireless capsule endoscopy images using textural features and svm-based feature selection. *Information Technology in Biomedicine, IEEE Transactions on*, 16(3):323–329, 2012.

[34] Michael Liedlgruber and Andreas Uhl. Computer-aided decision support systems for endoscopy in the gastrointestinal tract: A review. *IEEE reviews in biomedical engineering*, 4:73–88, 2011.

[35] David G Lowe. Distinctive image features from scale-invariant keypoints. *International journal of computer vision*, 60(2):91–110, 2004.

[36] J Mannath, V Subramanian, CJ Hawkey, and K Ragunath. Narrow band imaging for characterization of high grade dysplasia and specialized intestinal metaplasia in barrett's esophagus: a meta-analysis. *Endoscopy*, 42(05): 351–359, 2010.

[37] Frank Moosmann, Bill Triggs, and Frederic Jurie. Fast discriminative visual codebooks using randomized clustering forests. In *20th Annual Conference on Neural Information Processing Systems (NIPS'06)*, pages 985–992. MIT Press, 2007.

[38] Ruwan Nawarathna, JungHwan Oh, Jayantha Muthukudage, Wallapak Tavanapong, Johnny Wong, Piet C De Groen, and Shou Jiang Tang. Abnormal image detection in endoscopy videos using a filter bank and local binary patterns. *Neurocomputing*, 144:70–91, 2014.

[39] Nagaaki Ohyama, Hirohisa Machida, Kazuhiro Gono, Takashi Obi, Yasuo Hamamoto, Takao Endo, Masahiro Yamaguchi, Yasushi Sano, and Shigeaki Yoshida. Appearance of enhanced tissue features in narrow-band endoscopic imaging. *Journal of biomedical optics*, 9(3):568–577, 2004.

[40] Timo Ojala, Matti Pietikainen, and David Harwood. Performance evaluation of texture measures with classification based on kullback discrimination of distributions. In *Pattern Recognition, 1994. Vol. 1-Conference A: Computer Vision & Image Processing., Proceedings of the 12th IAPR International Conference on*, volume 1, pages 582–585. IEEE, 1994.

[41] Keiichi Onji, Shigeto Yoshida, Shinji Tanaka, Rie Kawase, Yoshito Takemura, Shiro Oka, Toru Tamaki, Bisser Raytchev, Kazufumi Kaneda, Masaharu Yoshihara, et al. Quantitative analysis of colorectal lesions observed on magnified endoscopy images. *Journal of gastroenterology*, 46(12):1382–1390, 2011.

[42] Konstantinos N Plataniotis and Anastasios N Venetsanopoulos. *Color image processing and applications*. Springer Science & Business Media, 2000.

[43] I Rácz and E Tóth. [chromoendoscopic study of the gastric mucosa]. *Orvosi hetilap*, 130(49):2635–2638, 1989.

[44] Farhan Riaz, Francisco Baldaque Silva, Mario Dinis Ribeiro, and Miguel Tavares Coimbra. Invariant gabor texture descriptors for classification of gastroenterology images. *Biomedical Engineering, IEEE Transactions on*, 59(10):2893–2904, 2012.

[45] Farhan Riaz, Francisco Baldaque Silva, Mario Dinis Ribeiro, and Miguel Tavares Coimbra. Impact of visual features on the segmentation of gastroenterology images using normalized cuts. *Biomedical Engineering, IEEE Transactions on*, 60(5):1191–1201, 2013.

[46] Lior Rokach. Fuzzy decision trees. 2008.

[47] R.R. Seeley, P. Tate, and T.D. Stephens. *Anatomy and Physiology*. McGraw-Hill Higher Education, 2007. ISBN 9780073293684.

[48] Jamie Shotton, Matthew Johnson, and Roberto Cipolla. Semantic texton forests for image categorization and segmentation. In *Computer vision and pattern recognition, 2008. CVPR 2008. IEEE Conference on*, pages 1–8. IEEE, 2008.

[49] MD Shui-Yi Tung, Cheng-Shyong Wu, and Ming-Yao Su. Magnifying colonoscopy in differentiating neoplastic from nonneoplastic colorectal lesions. *The American journal of gastroenterology*, 96:2628–2632, 2001.

[50] Rebecca Siegel, Jiemin Ma, Zhaohui Zou, and Ahmedin Jemal. Cancer statistics, 2014. *CA: a cancer journal for clinicians*, 64(1):9–29, 2014.

[51] Karen Simonyan, Andrea Vedaldi, and Andrew Zisserman. Descriptor learning using convex optimisation. *Computer Vision–ECCV 2012*, pages 243–256, 2012.

[52] R. Singh, GK Anagnostopoulos, K. Yao, H. Karageorgiou, PJ Fortun, A. Shonde, K. Garsed, PV Kaye, CJ Hawkey, K. Ragunath, et al. Narrow-band imaging with magnification in barrett's esophagus: validation of a simplified grading system of mucosal morphology patterns against histology. *Endoscopy*, 40(6):457, 2008.

[53] Rajvinder Singh, SweeLin Chen Yi Mei, and Sandeep Sethi. Advanced endoscopic imaging in barrett's oesophagus: A review on current practice. *World journal of gastroenterology: WJG*, 17(38):4271, 2011.

[54] MV Sivak. Gastrointestinal endoscopy: past and future. *Gut*, 55(8):1061–1064, 2006.

[55] Stephen M Smith and J Michael Brady. Susan—a new approach to low level image processing. *International journal of computer vision*, 23(1):45–78, 1997.

[56] Louis-Michel Wong Kee Song and Brian C Wilson. Endoscopic detection of early upper gi cancers. *Best Practice & Research Clinical Gastroenterology*, 19(6):833–856, 2005.

[57] Ricardo Sousa, Mario-Dinis Ribeiro, Pedro Pimentel-Nunes, and Miguel Tavares Coimbra. Impact of svm multiclass decomposition rules for recognition of cancer in gastroenterology images. pages 405–408, 2013.

[58] Ricardo Sousa, Daniel C Moura, Mario Dinis-Ribeiro, and Miguel T Coimbra. Local self similar descriptors: Comparison and application to gastroenterology images. In *Engineering in Medicine and Biology Society (EMBC), 2014 36th Annual International Conference of the IEEE*, pages 4635–4638. IEEE, 2014.

[59] Peter D Stevens, Charles J Lightdale, PH Green, Lance M Siegel, Reuben J Garcia-Carrasquillo, and Heidrun Rotterdam. Combined magnification endoscopy with chromoendoscopy for the evaluation of barrett's esophagus. *Gastrointestinal endoscopy*, 40(6):747, 1994.

[60] Venkataraman Subramanian and Krish Ragunath. Advanced endoscopic imaging: a review of commercially available technologies. *Clinical Gastroenterology and Hepatology*, 12(3):368–376, 2014.

[61] Xiaoyang Tan and Bill Triggs. Enhanced local texture feature sets for face recognition under difficult lighting conditions. *Image Processing, IEEE Transactions on*, 19(6):1635–1650, 2010.

[62] Thorsten Thadewald and Herbert Büning. Jarque–bera test and its competitors for testing normality–a power comparison. *Journal of Applied Statistics*, 34(1):87–105, 2007.

[63] JJW Tischendorf, S Gross, R Winograd, H Hecker, R Auer, A Behrens, C Trautwein, T Aach, and T Stehle. Computer-aided classification of colorectal polyps based on vascular patterns: a pilot study. *Endoscopy*, 42(03): 203–207, 2010.

[64] Tomasz Trzcinski, Mario Christoudias, Vincent Lepetit, and Pascal Fua. Learning image descriptors with the boosting-trick. In *Advances in neural information processing systems*, pages 269–277, 2012.

[65] Tinne Tuytelaars and Krystian Mikolajczyk. Local invariant feature detectors: a survey. *Foundations and Trends® in Computer Graphics and Vision*, 3(3):177–280, 2008.

[66] Vladimir Naumovich Vapnik and Vlamimir Vapnik. *Statistical learning theory*, volume 1. Wiley New York, 1998.

[67] Andreas Vécsei, Thomas Fuhrmann, Michael Liedlgruber, Leonhard Brunauer, Hannes Payer, and Andreas Uhl. Automated classification of duodenal imagery in celiac disease using evolved fourier feature vectors. *Computer methods and programs in biomedicine*, 95(2):S68–S78, 2009.

[68] Julia Vogel and Bernt Schiele. A semantic typicality measure for natural scene categorization. In *Pattern Recognition*, pages 195–203. Springer, 2004.

[69] Dag Wormanns, Martin Fiebich, Mustafa Saidi, Stefan Diederich, and Walter Heindel. Automatic detection of pulmonary nodules at spiral ct: clinical application of a computer-aided diagnosis system. *European radiology*, 12(5):1052–1057, 2002.

[70] Bangpeng Yao, Aditya Khosla, and Li Fei-Fei. Combining randomization and discrimination for fine-grained image categorization. In *Computer Vision and Pattern Recognition (CVPR), 2011 IEEE Conference on*, pages 1577–1584. IEEE, 2011.

[71] Naohisa Yoshida, Nobuaki Yagi, Yutaka Inada, Munehiro Kugai, Akio Yanagisawa, and Yuji Naito. Therapeutic and diagnostic approaches in colonoscopy. 2013.

[72] KC Yuan. Gastrointestinal cancer. *Journal of Gastrointestinal and Digestive System*, 3(125):2, 2013.

[73] Barbara Zitova and Jan Flusser. Image registration methods: a survey. *Image and vision computing*, 21(11): 977–1000, 2003.